Received: 1 July 2019 | Revised: 5 September 2019 | Accepted: 14 November 2019

DOI: 10.1002/cne.24820

RESEARCH ARTICLE

JCN RESEARCH IN SYSTEMS NEUROSCIENCE THE JOURNAL OF COMPARATIVE NEUROLOGY WILEY

Adult neurogenesis in crayfish: Origin, expansion, and migration of neural progenitor lineages in a pseudostratified neuroepithelium

Georg Brenneis[1,2] | Barbara S. Beltz[1]

[1]Wellesley College, Neuroscience Program, Wellesley, Massachusetts, USA

[2]Universität Greifswald, Zoologisches Institut und Museum, AG Cytologie und Evolutionsbiologie, Greifswald, Germany

Correspondence
Georg Brenneis, Universität Greifswald, Zoologisches Institut und Museum, AG Cytologie und Evolutionsbiologie, Soldmannstr. 23, 17489 Greifswald, Germany.
Email: georg.brenneis@gmx.de

Barbara S. Beltz, Wellesley College, Neuroscience Program, 106 Central Street, Wellesley, MA 02481, USA.
Email: bbeltz@wellesley.edu

Funding information
Deutsche Forschungsgemeinschaft, Grant/Award Numbers: BR5039/1-1, BR5039/3-1; National Science Foundation, Grant/Award Number: NSF-IOS-1656103

Peer Review
The peer review history for this article is available at https://publons.com/publon/10.1002/cne.24820.

Abstract

Two decades after the discovery of adult-born neurons in the brains of decapod crustaceans, the deutocerebral proliferative system (DPS) producing these neural lineages has become a model of adult neurogenesis in invertebrates. Studies on crayfish have provided substantial insights into the anatomy, cellular dynamics, and regulation of the DPS. Contrary to traditional thinking, recent evidence suggests that the neurogenic niche in the crayfish DPS lacks self-renewing stem cells, its cell pool being instead sustained via integration of hemocytes generated by the innate immune system. Here, we investigated the origin, division and migration patterns of the adult-born neural progenitor (NP) lineages in detail. We show that the niche cell pool is not only replenished by hemocyte integration but also by limited numbers of symmetric cell divisions with some characteristics reminiscent of interkinetic nuclear migration. Once specified in the niche, first generation NPs act as transit-amplifying intermediate NPs that eventually exit and produce multicellular clones as they move along migratory streams toward target brain areas. Different clones may migrate simultaneously in the streams but occupy separate tracks and show spatio-temporally flexible division patterns. Based on this, we propose an extended DPS model that emphasizes structural similarities to pseudostratified neuroepithelia in other arthropods and vertebrates. This model includes hemocyte integration and intrinsic cell proliferation to synergistically counteract niche cell pool depletion during the animal's lifespan. Further, we discuss parallels to recent findings on mammalian adult neurogenesis, as both systems seem to exhibit a similar decoupling of proliferative replenishment divisions and consuming neurogenic divisions.

KEYWORDS

adoptive transfer, BrdU, cell proliferation, EdU, nervous system, neural stem cell, *Procambarus clarkii*, RRID: AB_477585, RRID: AB_261811, RRID: AB_2338459, RRID: AB_2338914, RRID: AB_2341179, RRID: AB_2338362, RRID: AB_2338006, RRID: SCR_007370, RRID: SCR_014199, RRID: SCR_010279

1 | INTRODUCTION

Throughout most of the 20th century, the accepted view was that new neurons are generated only during embryonic and perinatal life in the vast majority of vertebrate and invertebrate organisms. Only after the introduction of S-phase specific in vivo markers that facilitated the tracking of cell proliferation and substantial improvements of immunohistochemical techniques, this dogma was finally discarded (see Gage & Temple, 2013) as functional integration of new neurons was demonstrated in adult brains of a variety of vertebrate taxa (e.g., Grandel & Brand, 2013), including humans (Eriksson et al., 1998). For a long time, however, elucidation of the lineage relationships among the neural progenitor cells (NPs) producing the adult-born neurons proved challenging (e.g., Zhao, Deng, & Gage, 2008), until recently, when first live-imaging approaches in mice have begun to provide a more comprehensive understanding (e.g., Pilz et al., 2018). In parallel with vertebrates, studies on invertebrates (predominantly arthropods) have assessed the presence of adult neurogenesis and investigated the underlying mechanisms (e.g., Simoes, & Rhiner, 2017).

Two decades after the first reports of persistent cell proliferation in the brains of juvenile and adult decapod crustaceans (Harzsch & Dawirs, 1996; Harzsch, Miller, Benton, & Beltz, 1999; Schmidt, 1997; Schmidt & Harzsch, 1999), this arthropod group has become an intensely studied model taxon for adult neurogenesis. The regions featuring life-long neurogenesis in the decapod brain are the lateral protocerebrum (optic neuropils and hemiellipsoid body; e.g., Schmidt, 1997; Sullivan & Beltz, 2005) and the deutocerebrum (for review, see Sandeman, Bazin, & Beltz, 2011; Wittfoth & Harzsch, 2018). In the latter, the deutocerebral proliferative system (DPS; sensu Wittfoth & Harzsch, 2018) generates adult-born neurons that integrate into the central olfactory pathway (e.g., Schmidt, 2001; Sullivan & Beltz, 2005). DPS anatomy is best understood in the spiny lobster *Panulirus argus* (e.g., Schmidt, 2007; Schmidt & Derby, 2011) and in crayfish (e.g., Sullivan, Benton, Sandeman, & Beltz, 2007; Chaves da Silva, Benton, Beltz, & Allodi, 2012), which have proved suitable for mechanistic studies.

In crayfish, the DPS forms during early postembryonic development (Sintoni, Benton, Beltz, Hansson, & Harzsch, 2012; Song, Johnstone, Edwards, Derby, & Schmidt, 2009). It is located on the ventral side of the deutocerebrum (Figure 1b) and comprises three anatomically confluent, yet morphologically distinguishable regions: (a) the neurogenic niche, (b) the migratory streams, and (c) the proliferation zones (Figure 1e). The niche lies on the surface of the accessory lobe and is a bilobed cluster of densely packed cells, the majority of which are bipolar (Type 1 cell sensu Zhang, Allodi, Sandeman, & Beltz, 2009). A short process of each Type 1 cell extends toward the niche's center, where they converge around a small cavity (Figure 1c–e; Sullivan et al., 2007; Chaves da Silva et al., 2012). A second, significantly longer process projects in the opposite direction across the accessory lobe's surface toward the medial neuron Cluster 9 (housing local interneurons) or lateral neuron Cluster 10 (housing projection neurons; Figure 1b,e). In each direction, these long Type 1 cell processes are tightly bundled, forming the so-termed migratory stream. Pulse-chase experiments with different in vivo cell proliferation markers that are incorporated into DNA of cells in S phase have demonstrated directed migration of NPs from the niche along the streams to the neuron clusters (Benton, Zhang, Kirkhart, Sandeman, & Beltz, 2011; Sullivan et al., 2007). In these clusters, NPs enter a proliferation zone in which mitoses occur on a regular basis (e.g., Zhang et al., 2009).

At the level of single adult NP lineages, the current DPS model proposes three spatially separated cell generations (Benton et al., 2011, 2014; Zhang et al., 2009). The first generation NPs in the niche do not self-renew in stem cell-like manner (Benton et al., 2011, 2014) but data suggested that they divide only once in a morphologically symmetric fashion before both of their daughter cells (= second generation NPs) start to migrate along the streams. The second generation NPs act as transit-amplifying cells, with some of these undergoing mitosis in the streams. The majority then enters M phase in the proliferation zones, where they subsequently divide at least once (= third generation) or potentially multiple times prior to cell cycle exit and neuronal differentiation (e.g., Zhang et al., 2009). One of the most intriguing aspects of this model is the lack of self-renewal in the first generation NPs. This contrasts not only with the embryonic NP lineages in crayfish, which feature asymmetrically dividing, self-renewing neural stem cells (neuroblasts) at their base (e.g., Scholtz, 1992; Sintoni et al., 2012; Sullivan & Macmillan, 2001). It also indicates replenishment of niche cells by an external source, as niche cell number increases with animal size despite continuous NP efflux and lack of additional niche divisions (Zhang et al., 2009). Notably, the DPS shows considerable vascularization (Chaves da Silva, Benton, Sandeman, & Beltz, 2013; Sullivan et al., 2007) and various lines of evidence support attachment and integration of hemocytes into the niche (Benton et al., 2011; Chaves da Silva et al., 2013) as well as their direct involvement in the production of new adult NP lineages (Benton et al., 2014).

Given the current lack of a live-imaging approach for the crayfish DPS, division and migration patterns of NP lineages and hemocyte–niche interactions cannot be observed directly but need to be reconstructed from fixed brain preparations. To some extent, such reconstructions are made challenging by the more flexible nature of adult neurogenesis compared to embryonic neurogenesis. Proliferation rates in the DPS decrease gradually with animal size (Zhang et al., 2009) but are also susceptible to a variety of other factors. For instance, NP proliferation and/or survival of the adult-born neurons have been shown to be regulated by endogenous levels of serotonin (Benton, Goergen, Rogan, & Beltz, 2008; Sandeman, Benton, & Beltz, 2009; Zhang, Benton, & Beltz, 2011), nitric oxide (Benton, Sandeman, & Beltz, 2007), and cytokines (Benton et al., 2014) and respond to environmental enrichment (Ayub, Benton, Zhang, & Beltz, 2011; Sandeman & Sandeman, 2000) as well as physical activity (Kim, Sandeman, Benton, & Beltz, 2014). This contrasts starkly with embryonic neurogenesis in crayfish and other malacostracan crustaceans, where the basic nervous system components are laid down by segmental NP lineages in a largely stereotyped division sequence (e.g., Ungerer & Scholtz, 2008).

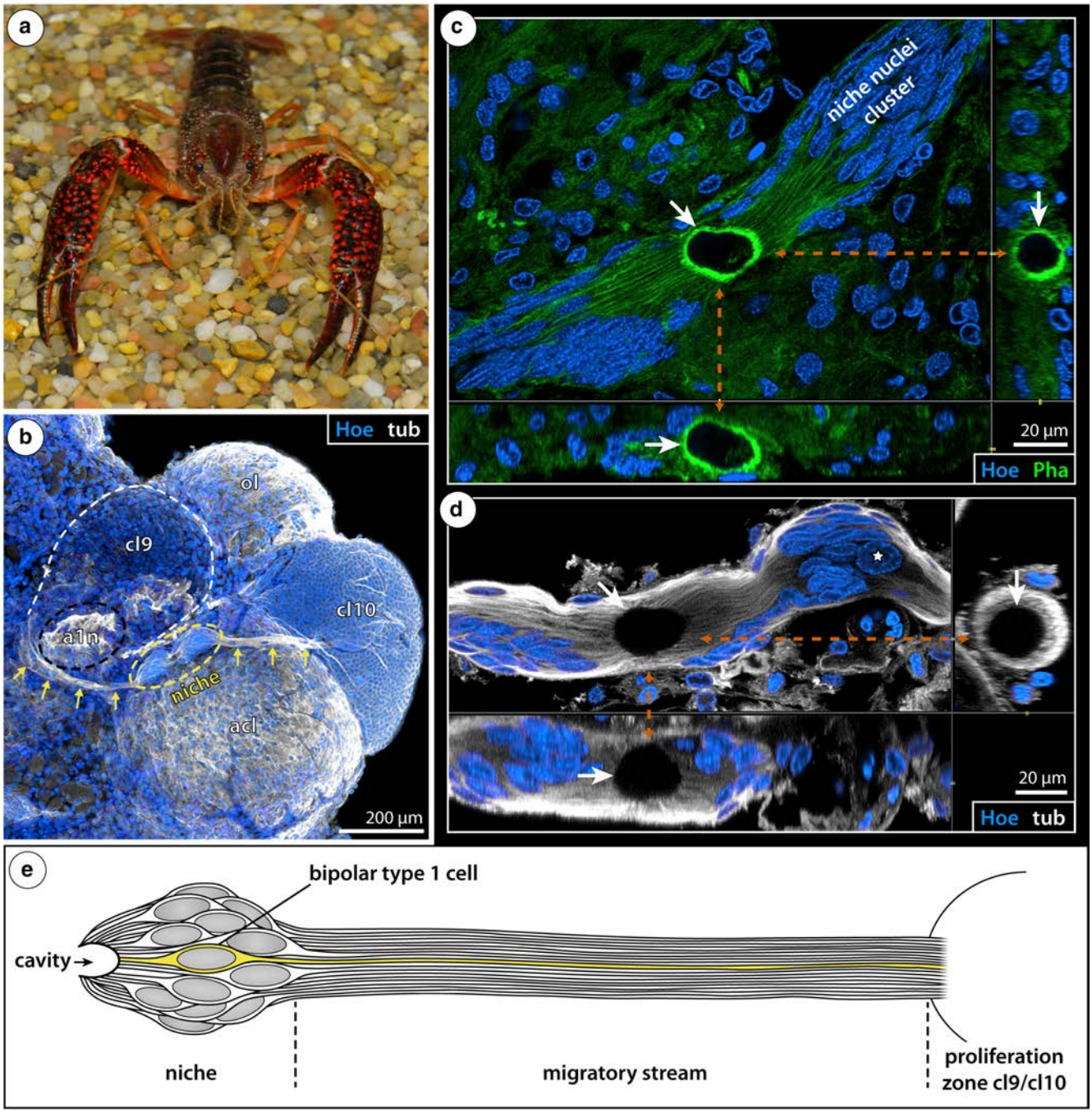

FIGURE 1 *Procambarus clarkii* and anatomy of its adult deutocerebral proliferative system (DPS). (a) Live male specimen of *P. clarkii*. (b) Ventral view of a desheated deutocerebral hemisphere, immunolabeling of acetylated tubulin (white) with nuclear counterstain (blue), maximum projection. The yellow stippled oval outlines the bilobed niche on the ventral surface of the accessory lobe (acl). Yellow arrows indicate the migratory streams toward neuron Clusters 9 and 10 (cl9 and cl10, respectively; cl9 highlighted by white stippled line). Note that the stream toward cl9 curves around the root of the antenna 1 nerve (a1n, black stippled oval). (c) Optical sections through a niche, phalloidin labeling (green) with nuclear counterstain (blue), Imaris section mode. Note strong F-actin signal in the apical tips of Type 1 niche cell processes (arrows) and the uncompressed cell-free cavity lumen as seen in the sagittal and cross sections shown at the right and bottom, respectively. (d) Optical sections through a niche, acetylated tubulin immunolabeling (white) with nuclear counterstain (blue), Imaris section mode. The centrally directed processes of the Type 1 niche cells outline the lumen of the uncompressed cell-free cavity (arrows). The star marks the nucleus of an enlarged first generation neural progenitor (NP). Note the extended unlabeled cytoplasm of the NP extending into the stream to the right. (e) Semi-schematic depiction of one half of the adult DPS. One of the Type 1 cells is highlighted in yellow to illustrate its bipolar extensions toward the niche cavity and the neuron clusters. Further abbreviations: ol, olfactory lobe [Color figure can be viewed at wileyonlinelibrary.com]

In the studies presented here, we examined more than 500 DPS preparations of *Procambarus clarkii* in order to shed more light on the cellular basis and migration patterns of the adult-born NP lineages. Samples were labeled for structural cytoskeletal proteins (tubulin and/or F-actin) as well as different combinations of markers for cell proliferation or mitosis. Special focus was put on the niche and migratory streams in search for consistently recurring cell patterns. We minimized artifacts caused by physical brain sectioning or tissue distortion via mounting of complete brains without *z*-axis compression, thus maintaining the natural spatial arrangements in the DPS. This was followed by documentation and detailed analysis of virtual three-dimensional (3d) stacks of more than 200 of the 500 DPS preparations. Using this setup, we provide evidence for (a) niche cell replenishment via limited numbers of intrinsic symmetric divisions with characteristics reminiscent of interkinetic nuclear migration, (b) slight morphological asymmetry of the first neurogenic divisions in the niche, (c) more actively proliferating transit-amplifying intermediate NPs than previously recognized, fueling the expansion of the adult neural lineages already during migration, (d) simultaneous migration of different NP clones, and (e) spatio-temporally flexible division patterns between clones as they migrate. Moreover, we present further indications for direct integration of hemocytes into the DPS. Based on our results, we develop a revised DPS model that highlights structural similarities to neuroepithelia in other arthropods and vertebrates and combines extrinsic cell replenishment via hemocytes with intrinsic niche cell amplification to explain the persistence of the neurogenic niche throughout the animal's lifespan. Further, this revised model also features interesting parallels to novel findings on adult neurogenesis in the mammalian brain in that it decouples cell replenishment divisions and consuming neurogenic divisions in the niche.

2 | MATERIALS AND METHODS

2.1 | Animal husbandry

Experiments were performed with the crayfish *P. clarkii* (Figure 1a). Animals were ordered from Carolina Biological Supply Company (Burlington, NC) and maintained in the Wellesley College Animal Care Facility at room temperature (RT) on a 12/12 light/dark cycle. They were kept in artificial pond water (double-distilled water with added trace minerals and sodium bicarbonate as a buffer) in aquaria and trays equipped with recirculating filter systems. Aquaria and trays contained gravel and some larger stones as well as plastic tubes and a few plastic plants as hiding spots. This enriched environment has been shown to promote high cell proliferation rates in the adult neurogenic system of procambarid crayfish (e.g., Ayub et al., 2011).

2.2 | Treatments of experimental animals

The data set analyzed in this study has been compiled from confocal microscopic scans of the DPS obtained during three different years (2015, 2017, and 2018). The animals studied covered varying sizes ranging from 10 mm to 45 mm carapace length (CL; measured from the posterior rim of the orbital cavity to the end of the carapace). Subgroups of these had been exposed to one of the following treatments prior to sacrifice, as they were originally contributing to several different experiments.

(a) Injection of crayfish saline (CS; 205 mM NaCl, 5.4 mM KCl, 34.4 mM $CaCl_2$, 1.2 mM $MgCl_2$, 2.4 mM $NaHCO_3$) containing fluorescently labeled dextran (Invitrogen™; 3,000 MW; micro-ruby or micro-emerald; #D7162 or #D7156, respectively) into the dorsal sinus 3–5 min prior to sacrifice;

(b) Injection of the in vivo cell proliferation markers 5-bromo-2′-deoxyuridine (BrdU; Sigma-Aldrich #B5002; 5 mg/ml) or 5-ethynyl-2′-deoxyuridine (EdU; provided in Click-iT® EdU Alexa Fluor® 488 Imaging Kit, Invitrogen—Molecular Probes® #C10337; 0.2 mg/ml) in CS at different time points before sacrifice (2, 3, 5, or 7 days);

(c) Injection of EdU or BrdU in 150–350 μl CS, followed by incubation for 5 or 7 days, respectively, and collection of 200–300 μl of hemolymph 5–10 min prior to sacrifice;

(d) Injection of BrdU- or EdU-labeled hemolymph in anticoagulation buffer (0.14 M NaCl, 10 mM EDTA, 30 mM trisodium citrate, 26 mM citric acid, 0.1 M glucose; pH 4.6) followed by varying postinjection time spans (3, 7, or 8 days; 3 or 4.5 weeks) prior to sacrifice.

Specimens subjected to the last two treatments were part of a series of adoptive transfer experiments in which proliferation marker-exposed hemolymph collected from donor animals (Treatment c) was injected into untreated recipient animals (Treatment d), in order to document the presence and location of marker-labeled cells in the DPS after the respective postinjection time of the recipients (see Benton et al., 2014 for more details).

An overview of the experimental treatments of specimens of which cellular DPS details are depicted in figures and movies are listed in Table 1.

2.3 | Dissection and fixation procedures

Irrespective of experiment, all animals were cooled in ice for 5–10 min prior to dissection. Next, the anterior part of the cephalothorax was cut off immediately and placed in cold 4% paraformaldehyde in phosphate-buffered saline (PBS; Boston BioProducts #BM-155). In order to guarantee swift penetration of the fixative into the tissues, the central brain was then removed from the "head" capsule. After 1–1.5 hr fixation at RT with gentle agitation on a horizontal shaker the neural sheath was carefully dissected from the brain, followed by immersion fixation overnight at 4°C. Only dextran-injected brains were not desheathed to avoid damage to delicate vasculature spanning between brain structures and the neural sheath. All brains were processed immunohistochemically after fixation, however, some underwent in-situ hybridization with DIG-labeled riboprobes prior to immunohistochemical labeling. In the present study, only the results of the immunohistochemical labeling procedures are reported.

TABLE 1 Experimental treatments of *Procambarus clarkii* specimens of which cellular details are shown in the figures and movies. See Section 2 for further treatment details

Figure/movie	CL [mm]	Experimental treatment prior to sacrifice and processing
1b	30–35	None
1c	Not documented	None
1d and 4h	35–45	Adoptive transfer donor—EdU injection 5 days prior to sacrifice
2a,b and 7e	40	BrdU injection 2 days prior to sacrifice
3a	30–35	Adoptive transfer recipient—Sacrifice 4,5 weeks post-transfer
3b	<15	None
3c	<15	None
3d	20–25	None
3e	10–12	Dextran injection
3f and 4c	30–35	Adoptive transfer donor—BrdU injection 7 days prior to sacrifice
3g	30–35	Adoptive transfer recipient—Sacrifice 4,5 weeks post-transfer
3h	35–45	Adoptive transfer donor—EdU injection 5 days prior to sacrifice
3i	35–45	Adoptive transfer donor—EdU injection 5 days prior to sacrifice
3j	25	BrdU injection 2 days prior to sacrifice
4a	30–35	Adoptive transfer recipient—Sacrifice 4,5 weeks post-transfer
4b and 6a	35–45	Adoptive transfer donor—EdU injection 5 days prior to sacrifice
4d	30–35	Adoptive transfer recipient—Sacrifice 3 days post-transfer
4e	30–35	Adoptive transfer recipient—Sacrifice 7 days post-transfer
4f	40	BrdU injection 2 days prior to sacrifice
4g	35–45	Adoptive transfer donor—EdU injection 5 days prior to sacrifice
5a	30–35	Adoptive transfer recipient—Sacrifice 7 days post-transfer
5b	30–35	Adoptive transfer recipient—Sacrifice 4,5 weeks post-transfer
5c	35–45	Adoptive transfer donor—EdU injection 5 days prior to sacrifice
5d,e	30–32	BrdU injection 2 days prior to sacrifice
5f	10	None
6b	35–45	Adoptive transfer donor—EdU injection 5 days prior to sacrifice
6c	30–35	Adoptive transfer recipient—Sacrifice 7 days post-transfer
6d	35–45	Adoptive transfer donor—BrdU injection 7 days prior to sacrifice
6e	35–45	Adoptive transfer donor—EdU injection 5 days prior to sacrifice
6f	35–45	Adoptive transfer donor—EdU injection 5 days prior to sacrifice
6g	30–35	Adoptive transfer recipient—Sacrifice 3 days post-transfer
7a	25–35	None
7b	25–35	None
7c	35–45	Adoptive transfer donor—EdU injection 5 days prior to sacrifice
7d	30–35	BrdU injection 5 days prior to sacrifice
8a	30–35	Adoptive transfer recipient—Sacrifice 7 days post-transfer
8b	30–35	Adoptive transfer recipient—Sacrifice 3 days post-transfer
8c,c′	25	BrdU injection 3 days prior to sacrifice
8d,d′	40	BrdU injection 2 days prior to sacrifice
9a	15–25	BrdU injection 2 days prior to sacrifice
9b	40	BrdU injection 2 days prior to sacrifice
9c	30–35	Adoptive transfer recipient—Sacrifice 3 days post-transfer
9d	30–35	Adoptive transfer recipient—Sacrifice 4,5 weeks post-transfer
10a,b	30–35	Adoptive transfer recipient—Sacrifice 3 weeks post-transfer
11a,b	10–12	Dextran injection
11c	10–12	Dextran injection
11d	35–45	Adoptive transfer donor—EdU injection 5 days prior to sacrifice
Movie S1	15–25	BrdU injection 2 days prior to sacrifice
Movie S2	35–45	Adoptive transfer donor—EdU injection 5 days prior to sacrifice
Movie S3 and S4	40	BrdU injection 2 days prior to sacrifice

2.4 | Immunohistochemistry and fluorescent histochemistry

Brains were thoroughly rinsed for at least 3 hr in several changes of PBS (1.86 mM NaH_2PO_4, 8.41 mM Na_2HPO_4, 17.5 mM NaCl; pH 7.4) at RT. Next, they were permeabilized with several changes of PBS + 0.3% Triton-X (PBTx) for ≥2 hr. All primary and secondary antibodies were diluted in PBTx; incubation times lasted from 24 hr (smaller brains) to 48–72 hr (larger brains) at 4°C.

Immunolabeling of acetylated α-tubulin or tyrosinated tubulin was used to detect cytoskeletal microtubules. Primary monoclonal mouse antibodies (anti-ac-α-tub IgG 2b Isotype, clone 6–11 B-1, Sigma-Aldrich #T6793, RRID:AB_477585, dilution 1:200; anti-tyrosinated tubulin, clone TUB-1A2, Sigma-Aldrich #T9028, RRID:AB_261811, dilution 1:500–1,000) were applied in conjunction with a Cy3- or Alexa Fluor®647-coupled secondary goat antibody (anti-mouse IgG (H + L), Jackson ImmunoResearch Labs #115-165-166, RRID:AB_2338459 (Cy3) & #115-605-166, RRID:AB_2338914 (A647), dilution 1:200). These antibody combinations enabled reliable visualization of the neurogenic niche with its central cavity and the compact bundles of the niche cell processes forming the migratory streams. BrdU-positive cells were detected with a monoclonal rat anti-BrdU primary antibody (clone BU1/75 [ICR1], Accurate Chemical & Scientific Corporation #OBT0030G, RRID:AB_2341179, dilution 1:50) and an Alexa Fluor®488-coupled goat anti-rat secondary antibody (IgG(H + L), Jackson ImmunoResearch Labs #112-545-167, RRID:AB_2338362, dilution 1:250). Cells in M phase were detected with a polyclonal rabbit anti-phosphorylated histone H3 antiserum (Upstate Biotechnology, Lake Placid, NY #07-492, dilution 1:200) used in conjunction with a Cy3-coupled goat anti-rabbit secondary antibody (IgG(H + L), Jackson ImmunoResearch Labs #111-165-144, RRID:AB_2338006, dilution 1:200). All antibody incubations were followed by rinses in PBTx for at least 4 hr at RT with gentle agitation on a horizontal shaker.

EdU-positive cells were detected with a Click-iT® EdU Alexa Fluor® 488 Imaging Kit (Invitrogen—Molecular Probes® #C10337) following the guidelines of the manufacturer's protocol but with an extended Click-iT® reaction time of 2–3 hr at RT.

F-actin labeling for visualization of the cortical cytoskeleton was performed with Alexa Fluor® 488 phalloidin (Invitrogen—Molecular Probes® #A12379, 1:50 in PBTx) overnight at 4°C. For nucleic acid (nuclear) counterstaining, Hoechst (H33342, Invitrogen Molecular Probes® #H1399, 1 μg/ml in PBS) was applied after all other labeling procedures. Incubation lasted at least 1 hr and was occasionally extended overnight at 4°C.

Nonspecific binding of secondary antibodies was tested by omission of primary antibodies. This resulted in complete loss of specific signal. However, occasionally hemocytes of the granular type (see Lin & Söderhäll, 2011), attaching to the brain's surface or located in the vasculature, exhibited nonspecific cytoplasmic labeling. Additionally, the azide-based labeling reaction for EdU detection occasionally resulted in weak staining of granular cytoplasm in untreated hemocytes. However, these patterns of nonspecific labeling did not impact data interpretation, as most markers of interest were localized in the nucleus (Hoechst, BrdU, EdU, PH3), and also the targeted structural markers with cytoplasmic location (tubulin, F-actin) show specific staining characteristics that are readily distinguished from the granular cytoplasmic hemocyte labeling.

Notably, immunohistochemical processing with the anti-PH3 antiserum (see above) resulted not only in the expected staining of mitotic profiles but also in nonspecific labeling of the cytoplasm of a few single cells (presumably hemocytes; see last results section for more details). It is currently unknown, to which nontarget antigen(s) this antiserum is binding.

2.5 | Mounting of samples

After final rinsing in PBS, brains were transferred into nonhardening Vectashield® Mounting Medium (Vector Laboratories, Inc. #H-1000) and placed on microscopic slides, ventral side facing upward toward the cover slip. To avoid sample compression, pieces of Surgident periphery wax with a diameter surpassing the dorsoventral extension of the brains were attached to the corners of the cover slips. The distance between cover slip and microscopic slide was adjusted under a stereomicroscope via gradual compression of the flexible spacers until the cover slip just touched the brain. As a result, the DPS on the ventral surface (Figure 1b) could be observed and imaged in whole-mounts with no or only minimal compression along its *z*-axis (Figure 1c,d).

2.6 | Data documentation, analysis, and presentation

In total, labeling patterns in more than 500 DPS preparations were checked with confocal laser scanning microscopy (cLSM), using a Leica DMI 6000 CS microscope coupled to a Leica TCS SP5 II scan unit. Out of these, a selection of more than 200 samples with interesting cellular patterns was imaged for 3d analysis. Based on the excitation spectra of the applied fluorochromes, a combination of UV laser (405 nm → Hoechst), argon laser (488 nm → Alexa Fluor® 488) and helium-neon laser (543 nm → Cy™3; 633 nm → Alexa Fluor® 647) was chosen.

The 3d reconstruction software Imaris, V7.0.0 (http://www.bitplane.com/Default.aspx, RRID:SCR_007370) was used for subsequent analyses. Within the Surpass and Section visualization modules of this program (e.g., Figure 1b–d, respectively), software tools were applied as previously described (e.g., Brenneis, Stollewerk, & Scholtz, 2013). Importantly, oblique slicers were used in the Surpass module in order to create a 3d-curved virtual section plane. This enabled visualization of cell arrangements along the curved brain surface in a single 2d projection (Figure 2). Global contrast and brightness values of some of the images were adjusted using Adobe Photoshop CS5 (RRID:SCR_014199). All figures were compiled with Adobe Illustrator CS5 (RRID:SCR_010279). Supporting Information movies were generated in Imaris (Animation module) and subsequently transformed into MP4-format using the freeware FormatFactory (http://www.pcfreetime.com).

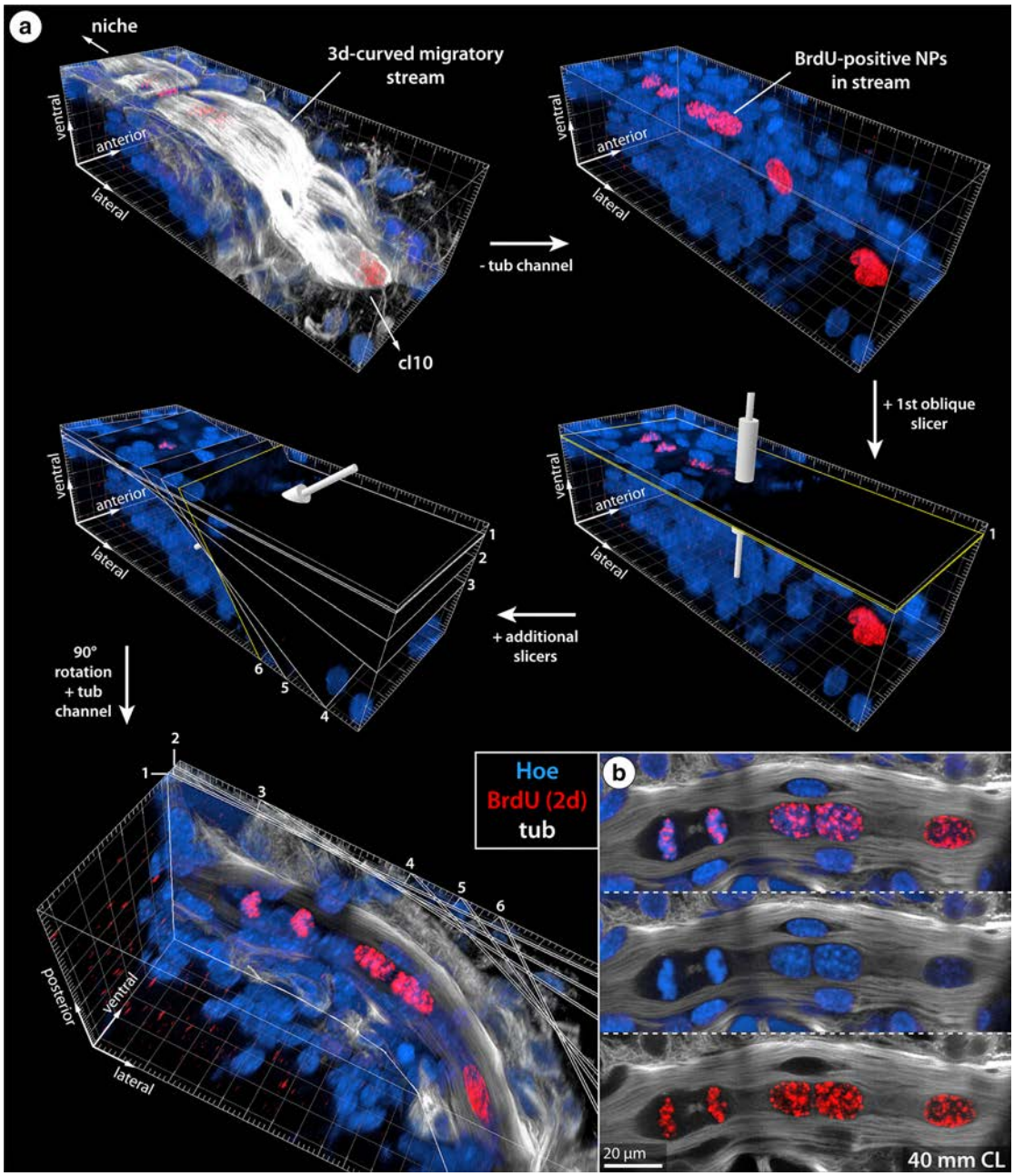

FIGURE 2 Creation of 3d-curved virtual section planes in Imaris. Acetylated tubulin and BrdU immunolabeling (white and red, respectively) coupled to nuclear counterstain (blue). Carapace length (CL) of specimen analyzed indicated in (b). (a) Sequence of steps to obtain a virtual section plane that follows the 3d-curvature of migratory stream in an uncompressed whole-mount brain of *Procambarus clarkii*. Starting from a 3d volume (Imaris Surpass mode) of the scanned portion of the migratory stream, oblique slicers are successively oriented along its course on the 3d-curved ventral surface of the accessory lobe. To control for correct slicer position, the 3d volume view can be deactivated while the slicers are being positioned. This allows flexible visualization of the structures included in the curved section that is being created and enables fine adjustment of slicer orientation. (b) 2d projection of the created 3d-curved virtual section (compare Figure 7e). A clone of four BrdU-positive NPs (one in telophase) is clearly visible as it migrates in the stream toward neuron Cluster 10 [Color figure can be viewed at wileyonlinelibrary.com]

3 | RESULTS

3.1 | Cell divisions in the niche and beginning migration of NPs

To visualize the niche and the exact dimensions of its central cavity, nuclear staining was coupled to phalloidin and/or tubulin labeling (Figure 1c,d). The latter two markers highlight the short processes of the Type 1 cells that form the inner cavity surface. Immunolabeling of the mitosis marker phosphorylated histone H3 was performed only in a subset of specimens (e.g., white arrow in Figure 3e), but advanced stages of M phase could also be reliably identified based on the nuclear staining (white arrows in Figure 3a–d,f–h). Further, tubulin labeling enabled detection of parts of the spindle apparatus or the

midbody that still spans between two sister cells prior to their final abscission (e.g., solid white arrowheads in Figure 3f–h,a,c–h).

While each of the more than 500 DPSs (in ~250 brains) processed in the course of the study has been checked with cLSM, ultimately not all of them were imaged and documented as virtual 3d stacks. In total, 3d stacks of 219 niches were obtained (Table 2). One of the imaging criteria for niches was the presence of mitotic profiles. Accordingly, the 47 niches with mitoses included in the niche data set (Table 2) represent approximately 10% of the DPSs checked in total.

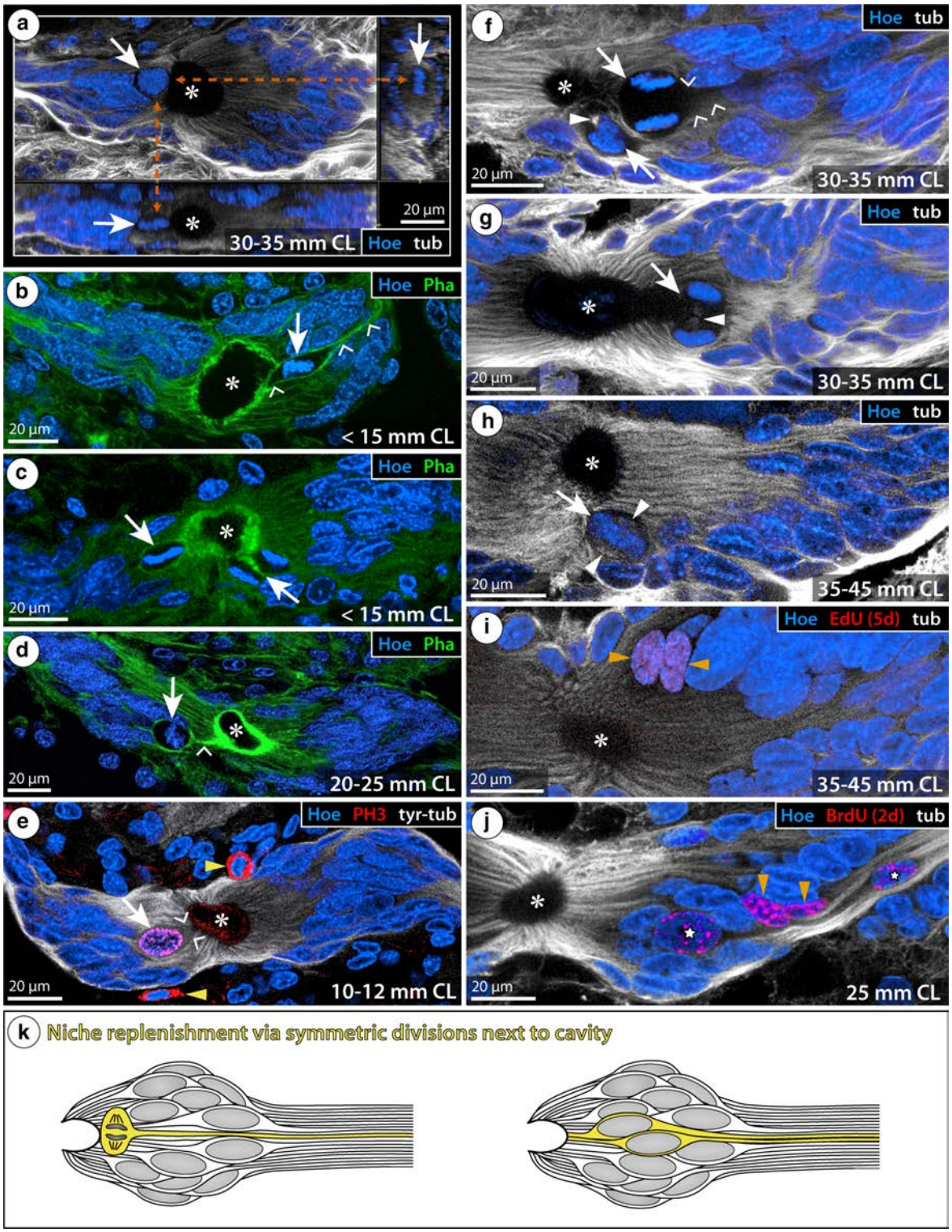

FIGURE 3 Legend on next page.

3.1.1 | Morphologically symmetric divisions occur next to the central niche cavity

Using the Imaris section mode, we analyzed the location and orientation of mitotic profiles in the niche data set in more detail (Figure 3a). In animals of all sizes, we found mitotic profiles near the central cavity (Table 2); these represent about half of the mitoses observed, found in roughly 5% of all DPSs checked. The mitotic profiles are located among the short processes of the Type 1 niche cells, either directly adjacent to the cavity lumen (white arrows in Figure 3a–c,f–h) or slightly set off from it (Figure 3d,e). Phalloidin staining revealed that the mitotic cells extend a F-actin-rich process toward the cavity (small open arrowheads in Figure 3b,d) and in the direction of the stream (Figure 3b), which is reminiscent of Type 1 niche cells (Figure 3k). Such cytoplasmic extensions were also occasionally discernible in tubulin-labeled M phase cells (small open arrowheads in Figure 3e).

The division plane of the majority of meta-, ana-, and telophase profiles was found to be oriented perpendicular to the surface of the cavity (81% of all mitoses next to cavity; Table 2), indicating that both sister cells will initially come to lie side by side next to the latter (e.g., Figure 3c,f–h). Based on late telophase profiles, the prospective two sister cells do not exhibit significant size differences. In line with the implied symmetry of the sister cells, we occasionally found directly adjacent proliferation marker-labeled pairs of cells in the niche that featured the elongate nuclear morphology typical for Type 1 niche cells (orange arrowheads in Figures 3i,j and 8c).

3.1.2 | The first divisions in the NP lineages show slight morphological asymmetry

In addition to cell divisions near the central cavity, further mitotic profiles occur among the densely packed Type 1 cell nuclei and more distally toward the niche-stream boundary (Figure 4a-f); these represent the other half of the mitoses documented in niches studied. The orientation of meta-, ana-, and telophase profiles in these regions reveal a cell division plane perpendicular to the niche-stream axis (i.e., in an approximate 90° angle to the division planes observed next to the cavity). Hence, daughter cells of these mitoses are going to be lined up along the cell migration pathway, which agrees with previous descriptions of NP divisions (Song et al., 2009; Zhang et al., 2009).

Tubulin immunolabeling shows slight size differences between the cytoplasmic volumes of the two forming sister cells, where the larger of the two is the one closer to the central cavity (Figure 4c–f). Morphological asymmetry of the divisions is further corroborated by pre-abscission cell pairs with a tubulin-labeled midbody (solid white arrowheads in Figure 4g,h), showing similar asymmetries of the surrounding cytoplasmic compartments but also differently sized new nuclei (Figure 4g,h). Proliferation marker labeling in both asymmetric nuclei, as observed in an EdU-exposed specimen, further support the sister cell relationship of these paired cells (Figure 4h).

Compared to the elongate nuclei of Type 1 cells, nuclei of the asymmetric sister cells are larger, more spherical and typically less intensely stained by nuclear markers. These characteristics and the orientation of the divisions unequivocally identify the cell pairs as part of the NPs described in previous studies (Benton et al., 2011; Song et al., 2009; Sullivan et al., 2007; Zhang et al., 2009; Figure 4i).

3.1.3 | NPs entering the migratory streams stay aligned with their relatives

About 90% of the more than 500 niches studied did not contain mitotic cells or pre-abscission sister cells with midbody. Nonetheless, NP pairs at a slightly later stage, that is, after initiation of migration into the streams, can be still frequently identified. The nuclei of these NP pairs are spherical to oval and typically larger than the Type 1 cell nuclei (NP nuclei labeled with stars in Figure 5a–e). As might be expected for actively proliferating NPs, they are often positively labeled in specimens that had been exposed to in vivo S phase

FIGURE 3 Replenishment divisions of niche cells next to the central cavity. (a–j) Optical sections through niches (Imaris section mode [a] or oblique slicers [b–j]). Neuron Cluster 10 (not shown) always to the right. Acetylated tubulin immunolabeling (white) or phalloidin labeling (green) coupled to nuclear counterstain (blue). Carapace length (CL) as indicated in each image. Asterisks highlight the cavity lumen. Arrows mark mitotic profiles. White solid arrowheads indicate parts of the tubulin-labeled spindle apparatus. Small open arrowheads highlight cytoplasmic cell processes. (a) Inspection of the sagittal and cross sections through the niche (right and bottom) allows identification of a metaphase profile next to the cavity. (b) The mitotic cell features cell processes toward cavity and stream. (c) A cell in metaphase (left arrow) and one in late telophase (right arrow) are found next to the cavity. (d) Note the mitotic cell's process toward the cavity. (e) Specimen injected with dextran (data not shown) with additional PH3 immunolabeling (red). A prophase is found next to the cavity. Note cytoplasmic labeling of two cells with small, intensely labeled nucleus next to the niche (yellow arrowheads). (f) A telophase is located to the right of the cavity. The lower arrow marks the new nucleus of one cell of a pair still connected by a midbody (solid arrowhead). Its sister cell lies further ventral to the section shown (see Figure 4c). (g) Note telophase with spindle apparatus/midbody next to the cavity. (h) Note metaphase profile with spindle apparatus. (i) Specimen injected with EdU (red) 5 days prior to sacrifice. A pair of EdU-positive nuclei (orange arrowheads) is found close to the cavity. (j) Specimen injected with BrdU (red) 2 days prior to sacrifice. A pair of adjacent BrdU-positive Type 1 cell nuclei (orange arrowheads) is embedded in the niche cell cluster. Stars highlight BrdU-positive nuclei of an NP pair that are connected by a widened cytoplasmic track. Note the size difference between the two NPs. (k) Semi-schematic depiction of a symmetric replenishment division of a Type 1 niche cell with its division plane oriented perpendicular to the surface of the cavity [Color figure can be viewed at wileyonlinelibrary.com]

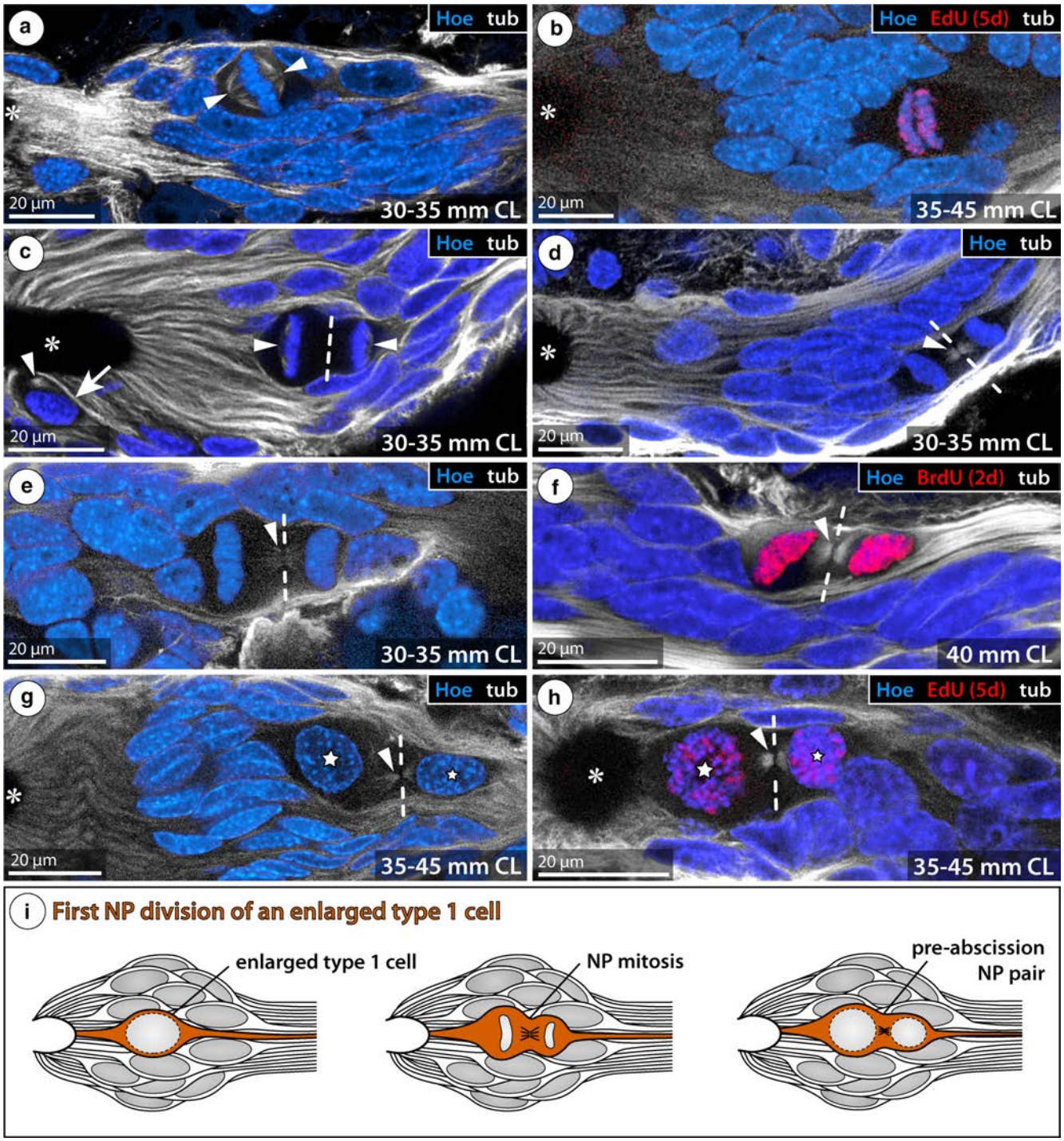

FIGURE 4 First division of activated neural progenitors (NPs) in the niche. (a–h) Optical sections through niches (Imaris oblique slicers). Cavity (asterisk) always oriented to the left. Acetylated tubulin immunolabeling (white) with nuclear counterstain (blue). Carapace length (CL) as indicated in each image. Solid arrowheads indicate parts of the tubulin-labeled spindle apparatus or midbody (a, c–h). Stippled lines highlight the position of the division plane as indicated by the spindle apparatus/midbody and/or the cytoplasmic outline of the dividing cell. (a) A NP in metaphase is present in the ventral layer of the niche cell cluster. (b) Specimen injected with EdU (red) 5 days prior to sacrifice. An EdU-positive NP in anaphase is found close to the niche-stream boundary. (c) A NP in telophase is located in the ventral layer of the niche cell cluster. Note the slight asymmetry of the cytoplasmic compartments surrounding the two prospective daughter cells. The arrow marks the new nucleus of a daughter cell of a replenishment division that still features the midbody (arrowhead). Its sister cell lies further dorsal to the section shown (see Figure 3f). (d) Note NP in telophase close to the niche-stream boundary. (e) Note slightly asymmetric telophase of an NP close to the niche-stream boundary. (f) Specimen injected with BrdU (red) 2 days prior to sacrifice. A slightly asymmetric division of a BrdU-positive NP is found at the outer edge of the niche cell cluster. (g) A NP pair (stars) with asymmetric nuclei is present close to the niche-stream boundary. The cell pair is still connected by its midbody (arrowhead). (h) Specimen injected with EdU (red) 5 days prior to sacrifice. A NP pair (stars) with midbody (arrowhead) and asymmetric EdU-positive nuclei is found centrally in the niche cell cluster, close to the cavity. (i) Semi-schematic depiction of an enlarged first generation NP and its slightly asymmetric first division with cleavage plane perpendicular to the niche-stream axis [Color figure can be viewed at wileyonlinelibrary.com]

TABLE 2 Descriptive statistics of different niche characteristics analyzed. The category "advanced mitotic profiles" subsumes meta-, ana-, and telophases

Category	Number or proportion
Niches documented with cLSM (virtual 3d stacks)	219[a]
Niches with large spherical nuclei of active NPs (mostly single, rarely > 1)	160/219 (73%)
Niche cavities with cell(s) inside lumen	0/219 (0%)
Niches with mitotic profiles (incl. sister cells with midbody)	47
Niches with mitotic profiles—sorted by treatment prior to sacrifice	
None	10
Injection of BrdU, EdU or dextran in CS	9
Injection of BrdU or EdU in CS + hemolymph-bleeding (AT donors)	15
Injection of donor hemolymph at different time points (AT recipients)	13
Mitoses next to the cavity / niches with mitotic profiles	24/47 (51%)
Mitoses next to the cavity / niches with mitotic profiles—sorted by animal size	
<25 mm CL	6/7 (86%)
25–35 mm CL	9/16 (56%)
35–45 mm CL	8/18 (44%)
Undocumented CL	1/6 (17%)
Advanced mitotic profiles/mitoses next to the cavity	16/24 (67%)
Perpendicular division plane to cavity/ advanced mitotic profiles next to cavity	13/16 (81%)

[a]The 219 niches were selected from more than 500 DPSs checked with cLSM.

markers (Figure 5d,e). Notably, both nuclei are located along a widened linear track with lower tubulin content, which extends along the niche-stream axis (small open arrowheads in Figure 5a–f). Phalloidin co-labeling reveals F-actin-rich cortical cytoskeleton to outline this widening, indicating that it represents extended cytoplasm of the NP sisters (Figure 5f). Further, phalloidin labeling highlights the position of the cell border between them (solid white arrowheads in Figure 5f). The NP closer to the cavity often possesses a slightly larger nucleus and a more voluminous cytoplasm (Figures 3j and 5b,c,f) but the observed size differences between both cells varied between samples (compare, e.g., Figure 5a,b,d,e). The NP nucleus further away from the niche was found at varying distances from the latter, suggestive of its active migration into the streams.

In carefully oriented optical sections, it was sometimes possible to trace a cytoplasmic projection of the larger NP all the way to the cavity lumen (Figure 5b). Also along the streams, the extended cytoplasm of the smaller NP could be followed for some distance (Figure 5a,d).

Notably, not every niche contains enlarged nuclei of active NPs (73% of the 3d-documented niches; Table 2). Further, when present, typically only a single enlarged NP or one NP pair aligned along the niche-stream axis is found per niche half. Only rarely, more than one NP/NP pair is encountered in one niche half (Figure 5f).

3.2 | Migration and expansion of NP lineages along the streams

More advanced stages of NP lineages were found along the migratory streams. The majority of observations were made in the stream leading to Cluster 10 (Figures 6–8), as it is easily observable and follows a comparably straight course on the ventral side of the accessory lobe. However, similar processes seem to occur in the stream toward Cluster 9 that curves around the root of the antenna 1 nerve and is not as readily visualized (Figure 9).

3.2.1 | Multicellular clones of NPs migrate along the streams

In a specimen exposed to EdU (5 days survival time), we identified a labeled NP in anaphase at the niche-stream border, together in a single widened track with another EdU-positive cell further distally in the stream (Figure 6a). This shows that after the first NP division in the niche, the daughter cell closer to the cavity may divide again before migration into the streams. Such additional divisions would be expected to generate linearly arrayed cell clones in the streams, comprising three cells or even more (in case of multiple divisions). Indeed, such strings of multiple cells can be observed (Figures 6b–f and 7), frequently showing proliferation marker labeling in specimens that were exposed to BrdU or Edu over several days (Figures 6d,e and 7c–e; Movie S1). Distances between the NP nuclei within linear clones were found to vary. In some cases, the two NPs nearest to the niche are close to each other, often with signs of nuclear asymmetry, which points to their recent division (Figure 6b,c,f; Movie S1). In other cases, their two nuclei are well-separated and of oval shape, suggestive of faster migration of the more distal cell after a division (Figures 6d,e and 7b). In the distal stream (closer to the proliferation zone associated with neuron Cluster 10), however, cells of a clone may be more tightly packed (Figure 7a–d). These varying patterns indicate

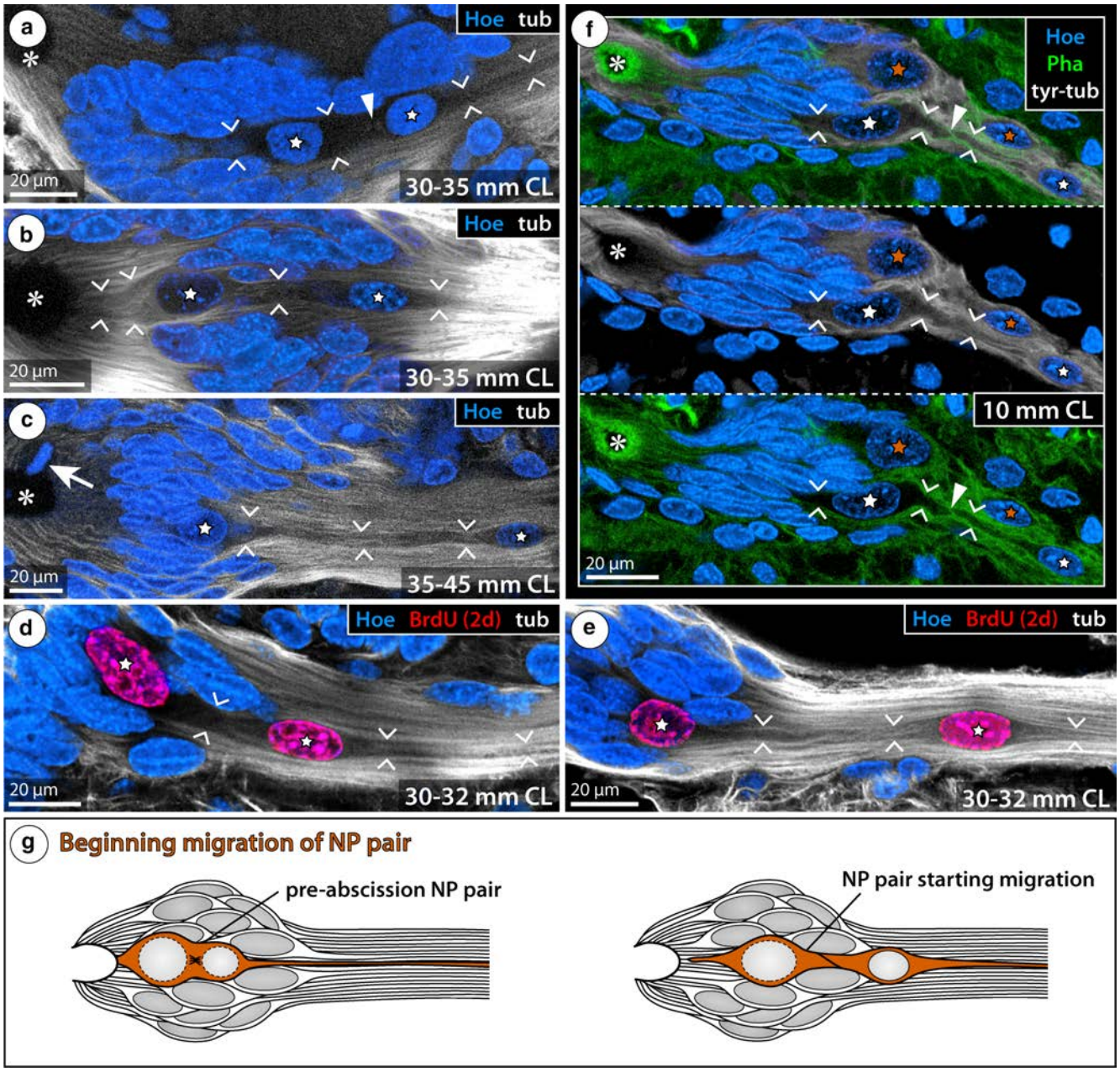

FIGURE 5 Beginning migration of NPs into the migratory streams. (a–f) Optical sections through niches (Imaris oblique slicers). Specimens of different carapace length (CL; indicated in each image); cavity (asterisk) always oriented to the left. Acetylated or tyrosinated tubulin immunolabeling (white) or phalloidin labeling (green) coupled to nuclear counterstain (blue). Stars mark the nuclei of two NP sister cells. Small open arrowheads highlight linear track of widened cytoplasm connecting the NPs as well as their cytoplasmic processes to the cavity and into the stream. (a) An NP pair with weakly tubulin-labeled midbody (solid arrowhead) is located close to the niche-stream boundary. (b) An asymmetric NP sister cell pair is found in the center of the niche cell cluster. Note the larger NP's widened cytoplasmic process to the cavity. (c) The smaller NP of an asymmetric sister cell pair has already migrated for some distance along the stream. The arrow marks a metaphase profile of a replenishment division next to the cavity. (d) Specimen injected with BrdU (red) 2 days prior to sacrifice. A BrdU-positive, asymmetric NP pair is found at the niche-stream boundary. (e) Specimen injected with BrdU (red) 2 days prior to sacrifice. One cell of the BrdU-positive NP pair has started migration into the stream. (f) Specimen double-labeled for tyrosinated tubulin and phalloidin; both labels shown in combination and separately with nuclear counterstain. Note that two asymmetric NP pairs (white and red stars) are found close the niche-stream boundary at the same time. F-actin surrounds the weakly tubulin-labeled, voluminous cytoplasm of the NP pair highlighted with white stars. The solid white arrowhead indicates the presumptive cell border between the two sister cells. (g) Semi-schematic depiction of beginning NP migration from the niche into the stream [Color figure can be viewed at wileyonlinelibrary.com]

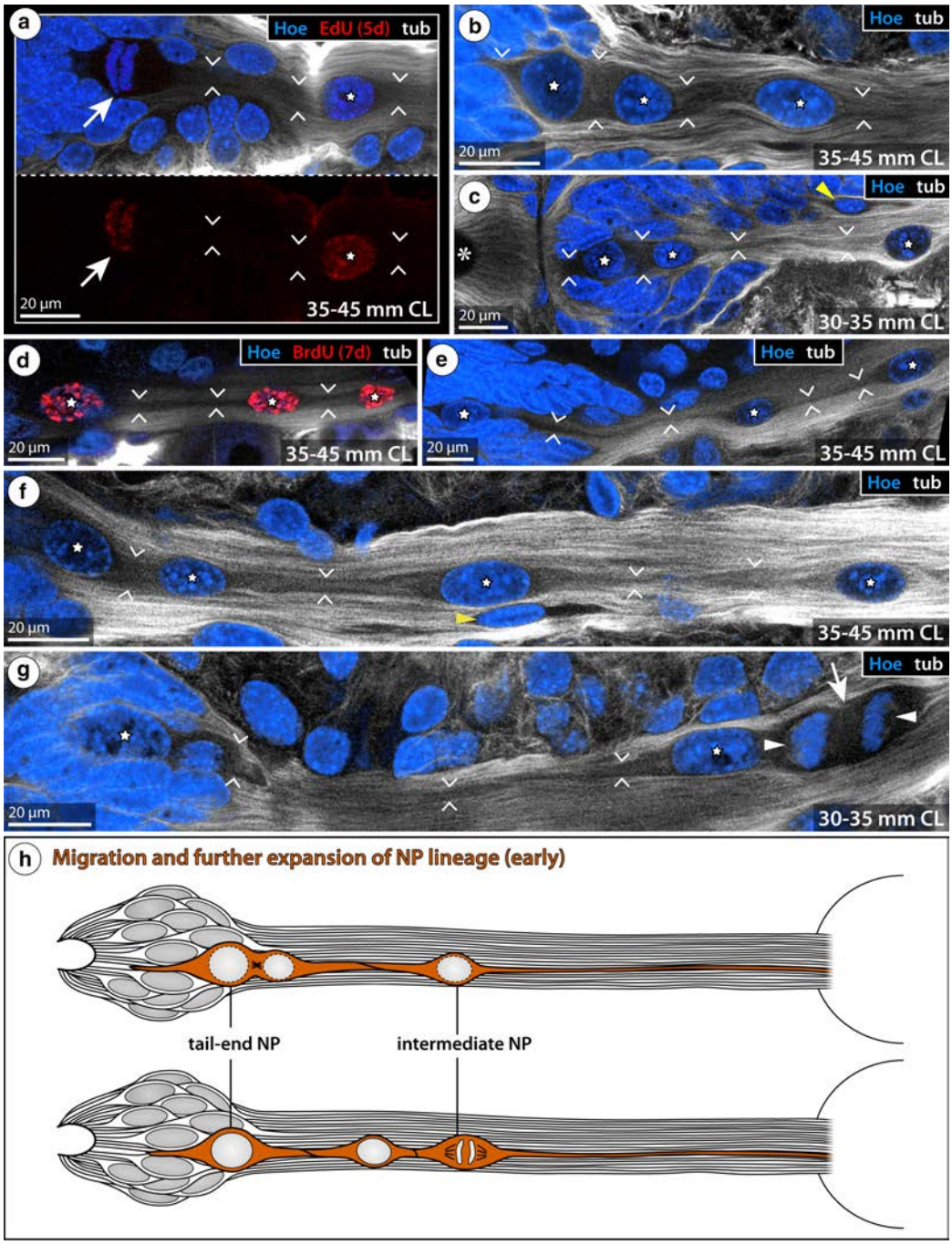

FIGURE 6 Expansion of NP lineages in early stages of migration. (a–g) Optical sections through niches and proximal stream portion (Imaris oblique slicers); cavity (asterisk) always oriented to the left, that is, NPs migrate toward the right. Acetylated tubulin immunolabeling (white) coupled to nuclear counterstain (blue). Carapace length (CL) as indicated in each image. Stars mark the nuclei of migrating NPs. Small open arrowheads highlight linear track of widened cytoplasm connecting NPs and their cytoplasmic processes further distally into the stream. (a) Specimen injected with EdU (red) 5 days prior to sacrifice; same specimen as in Figure 3b. The weak EdU signal of the NP in anaphase (arrow) and its migrating sister cell (star) are shown separately. (b) Three closely spaced NPs have started migration along the stream. (c) NP clone comprising three cells, one having started migration into the stream. Note slightly larger nucleus of the tail-end NP as compared to its presumptive sister cell directly ahead. Note also larger NP nucleus at the migration front. The small elongate nucleus (yellow arrowhead) of an unidentified cell type is found at the outer stream edge. (d) Specimen injected with BrdU (red) 7 days prior to sacrifice. NP clone comprising three cells. Note the larger nucleus of the tail-end NP. (e) NP clone comprising three well-separated cells, two having started migration into the stream. (f) NP clone comprising four well-separated cells. Note slightly larger nucleus of the tail-end NP as compared to its presumptive sister cell ahead. Note also larger NP nucleus ahead of the latter. The yellow arrowhead marks the small elongate nucleus of an unidentified cell type at the outer stream edge. (g) NP clone comprising three cells, the one at the migration front in telophase (arrow; arrowheads mark the tubulin-positive spindle apparatus). Due to the 3d curvature of niche and stream, the cytoplasmic connection between the large tail-end NP among the niche cells and the migrating NPs in the stream cannot be completely traced in this single section. (h) Semi-schematic model of the ongoing expansion of a NP lineage at an early stage of migration, including divisions of tail-end NP but also in intermediate NPs closer to the migration front [Color figure can be viewed at wileyonlinelibrary.com]

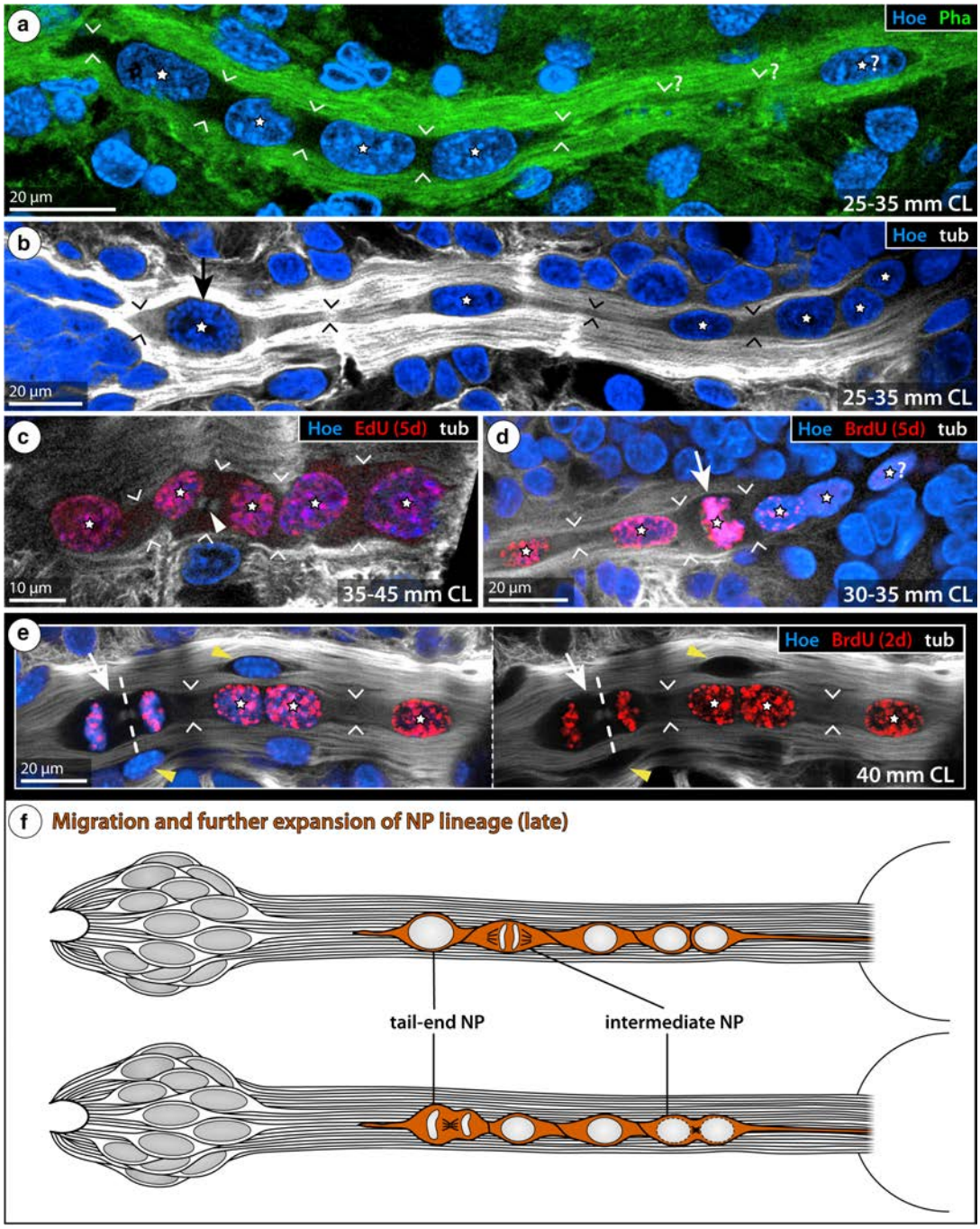

FIGURE 7 Further expansion of NP lineages in more advanced stages of migration. (a–e) Optical sections through migratory streams (Imaris oblique slicers). The niche is located to the left, that is, NPs migrate toward the right. Acetylated tubulin immunolabeling (white) or phalloidin labeling (green) coupled to nuclear counterstain (blue). Carapace length (CL) as indicated in each image. Stars mark the nuclei of migrating NPs. Small open arrowheads highlight linear track of widened cytoplasm connecting NPs and their cytoplasmic processes further distally into the stream. (a) A clone comprising four closely spaced NPs migrates along the stream. A fifth cell further ahead seems to be part of the same clone but the connecting track is not distinctly traceable in this section. (b) A clone comprising at least six NPs. Note enlarged nucleus of the tail-end NP (arrow), which is presumably in prophase given the typical punctate DNA structure that cells in prophase generally have. The NPs closer to the neuron cluster feature more roundish nuclei. (c) Specimen injected with EdU (red) 5 days prior to sacrifice. Clone of five EdU-positive NPs in a stream portion close to the neuron cluster. One NP sister cell pair is still connected by its midbody (white arrowhead). (d) Specimen injected with BrdU (red) 5 days prior to sacrifice. Part of a NP clone entering into Cluster 10. Note metaphase profile (arrow) of one BrdU-positive NP. (e) Specimen injected with BrdU (red) 2 days prior to sacrifice. Clone of four BrdU-positive NPs. Note that the tail-end NP is in telophase (arrow). The stippled line marks the presumptive division plane as indicated by the spindle apparatus/midbody. Yellow arrowheads mark small elongate nuclei of two unidentified cells at the outer stream edges. Omission of the nuclear counterstain (right image) shows that these elongate cells are completely BrdU-negative. (f) Semi-schematic model of the expansion of a clone in an advanced stage of migration, including divisions of the tail-end NP and of intermediate NPs closer to the migration front [Color figure can be viewed at wileyonlinelibrary.com]

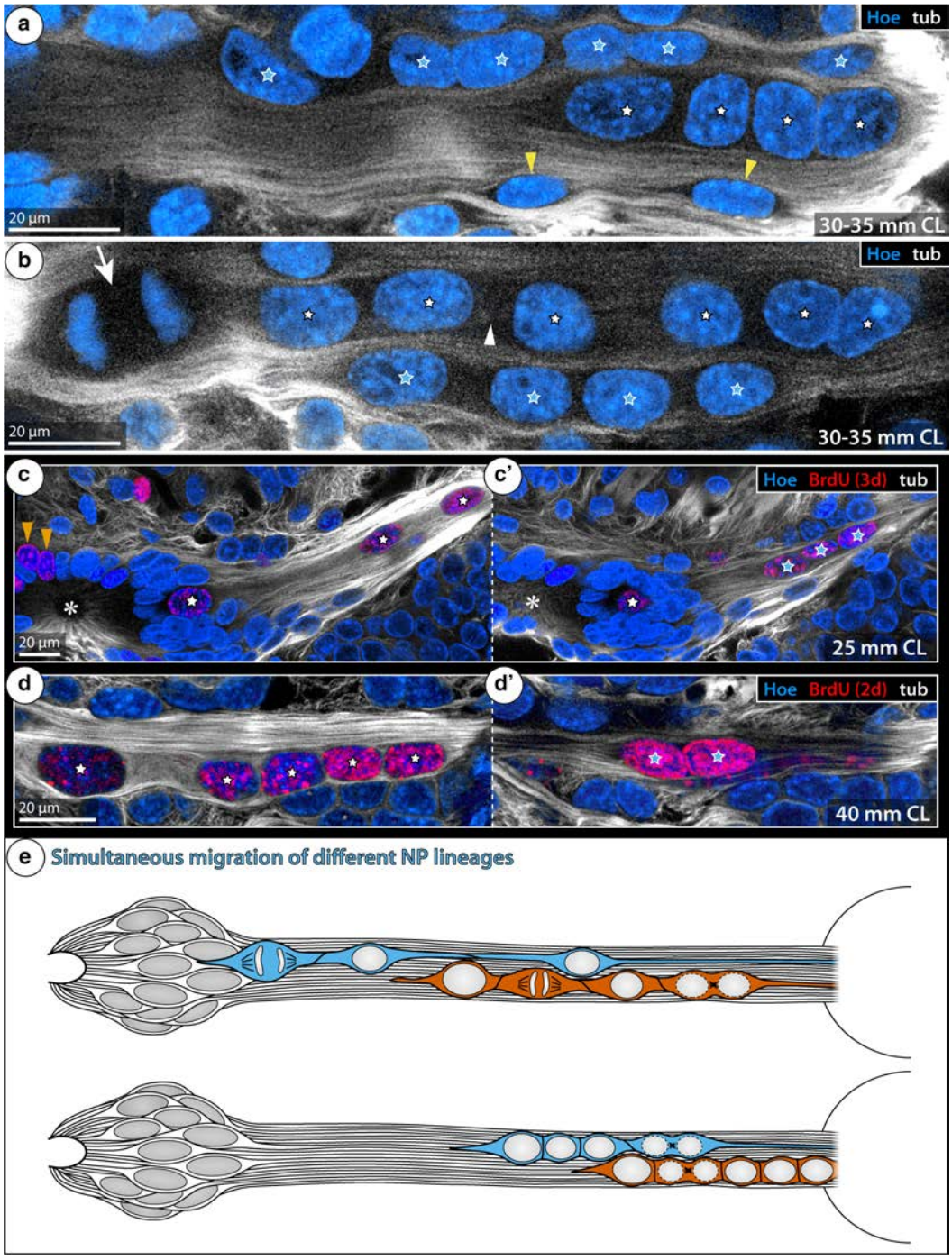

FIGURE 8 Simultaneous migration of different NP lineages along the stream. (a–d′) Optical sections through niche and/or migratory streams (Imaris oblique slicers). The niche is located to the left, that is, NPs migrate toward the right. Acetylated tubulin immunolabeling (white) coupled to nuclear counterstain (blue). Carapace length (CL) as indicated in each image. Stars mark the nuclei of migrating NPs; differently colored stars indicate different clones. (a) Two NP clones migrate in parallel along the stream. Note differences in the cell number and nuclear shapes between the clones. Yellow arrowheads mark smaller elongate nuclei of a pair of two unidentified cells at the outer stream edge. (b) Two simultaneously migrating NP clones in the stream. Note that the tail-end NP of the more expansive clone is in telophase (arrow). The white arrowhead highlights the weakly tubulin-labeled midbody of a sister cell pair further ahead in the same clone. (c,c′) Specimen injected with BrdU (red) 3 days prior to sacrifice; c lies directly ventral to c′ but with slightly different angle of the oblique slicer. The asterisk marks the position of the niche cavity. (c) A BrdU-positive NP clone comprising three cells has started migration in the ventral stream layer. Orange arrowheads mark two adjacent EdU-positive Type 1 cell nuclei next to the cavity. (c′) Another three-cell-clone migrates directly dorsal to the clone shown in c (note that the dorsal portion of the latter's tail-end NP is still visible in this section). (d,d′) Specimen injected with BrdU (red) 2 days prior to sacrifice. Stream toward Cluster 9, where d is directly ventral to d′. (d) A BrdU-positive NP clone comprising five cells migrates in the ventral stream layer. Note the large nucleus of the tail-end NP. (d′) Two BrdU-positive NPs of a different clone are found directly dorsal to the five-cell-clone shown in d (note scattered specks of BrdU-signal of the latter shining through). (e) Semi-schematic sketch of the simultaneous migration of two different NP clones along the stream [Color figure can be viewed at wileyonlinelibrary.com]

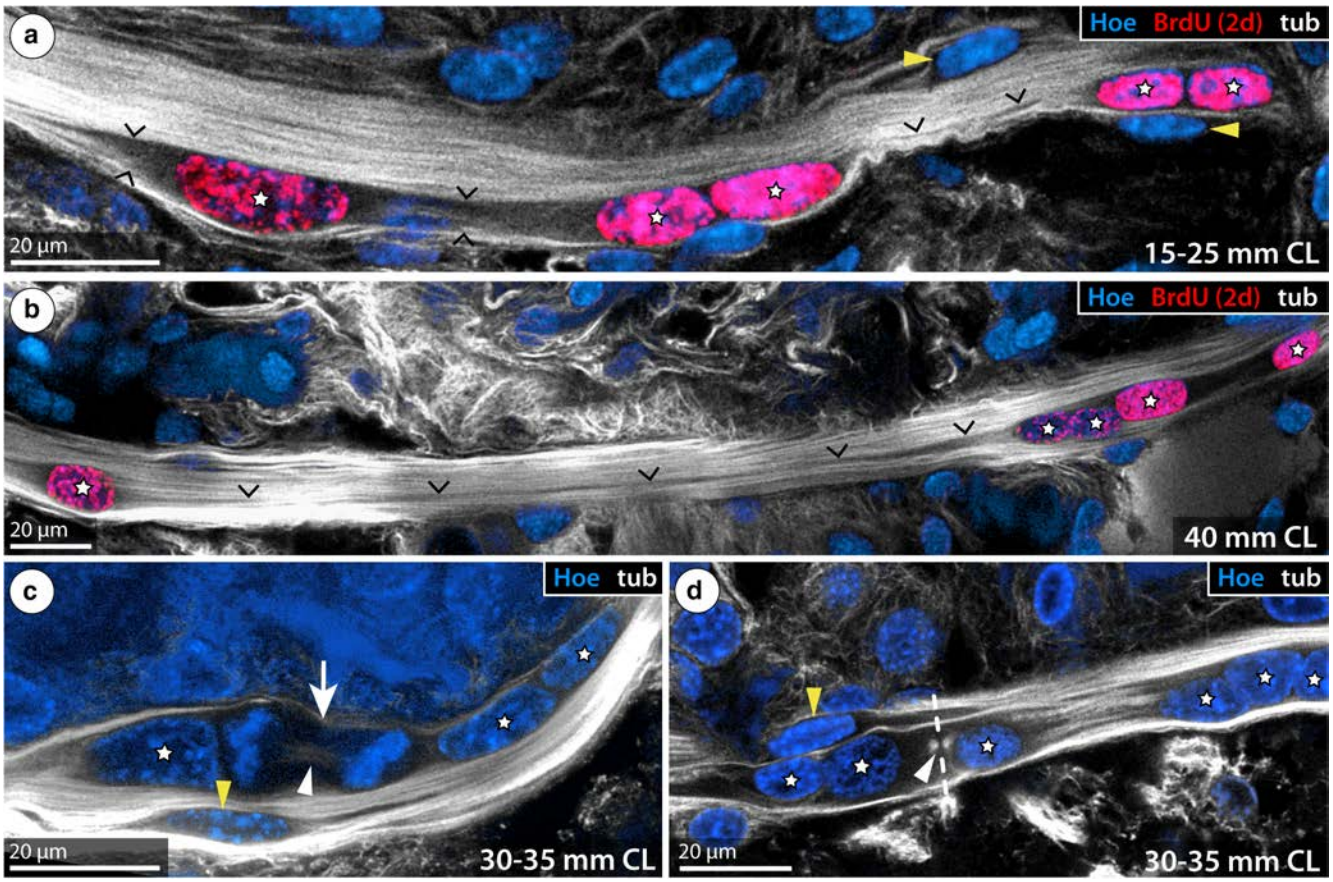

FIGURE 9 NP clones migrating toward Cluster 9. (a–d) Optical sections through migratory streams (Imaris oblique slicers). The niche is located to the left, that is, NPs migrate toward the right. Acetylated tubulin immunolabeling (white) coupled to nuclear counterstain (blue). Carapace length (CL) as indicated in each image. Stars mark nuclei of migrating NPs. Small open arrowheads highlight linear track of widened cytoplasm connecting the NPs and their cytoplasmic processes along the stream. (a) Specimen injected with BrdU (red) 2 days prior to sacrifice. Five BrdU-positive NPs of one clone migrate toward Cluster 9. Note the large nucleus of the tail-end NP and the paired arrangement of the four NPs ahead of it (potential sister cell pairs). Two cells with elongate nuclei (yellow arrowhead) are found at the outer edges of the stream. (b) Specimen injected with BrdU (red) 2 days prior to sacrifice. Five BrdU-positive NPs migrate toward Cluster 9. Note the considerable distance between the tail-end NP and the next nuclei ahead, but the persisting narrow linear track (small arrowheads) between them. (c) A NP clone comprising four cells is highlighted. The intermediate NP directly ahead of the tail-end NP passes through telophase (arrow). The spindle apparatus is tubulin-labeled (white solid arrowhead) and the positions of the newly forming nuclei seems to indicate a slight morphological asymmetry even in this intermediate NP division. Note a single cell with elongate nucleus (yellow arrowhead) at the outer edge of the stream. (d) A NP clone comprising at least six cells is shown. One sister cell pair is still interconnected by the tubulin-positive midbody, the position of which (stippled line) and the slightly differently sized nuclei indicating morphological asymmetry of the preceding division. Next to the clone, a single unidentified cell with elongate nucleus (yellow arrowhead) is found at the outer edge of the stream [Color figure can be viewed at wileyonlinelibrary.com]

temporally dynamic cell migration within clones, that is, the migration speed of single NPs seems to fluctuate over time and there is no apparent coordination within a clone.

Notably, in clones of three or more cells, not only the NP closest to the niche (arrows in Figures 7b,e and 8b) but also cells further ahead were observed in mitosis (e.g., arrows in Figures 6g, 7c,d and 9c). Accordingly, migrating clones encompass additional proliferating NPs that contribute to lineage expansion in addition to the niche-end NP. In light of this, nuclear size differences within such multicellular clones (e.g., Figures 6b,c,f and 7b) may be attributable to NPs passing through G phases. Similarly, more closely spaced cell pairs in a multicellular clone may indicate a recent division of an NP. This latter interpretation finds some support in the comparable signal intensity of proliferation markers in such pairs (e.g., Figures 7e, 8d,d′ and 9a,b) and may account for previous reports of NP migration in cell pairs along the streams (Zhang et al., 2009).

3.2.2 | Multiple clones can migrate at the same time along the streams

We also encountered more complex cell patterns in some of the streams studied (Figure 8). Their 3d analysis revealed the simultaneous occurrence of more than one linear cell clone along a migratory stream. In these cases, different clones occupy separate “lanes” in the stream, positioned either side by side (Figure 8a,b) or in different dorso-ventral planes (Figure 8c–d′; Movie S2). More distally, where the stream starts to dive into the more dorsal proliferation zone inside Cluster 10, we

observed a maximum of three such cell clones aligned side by side (Movie S3). In one instance, we also detected two clones "switching sides" in different dorso-ventral planes, matching the equally spiraling course of the cell processes constituting the stream in the specimen (Movie S4). Accordingly, instead of a simple linear system, the streams rather represent multi-lane highways along which different separate NP lineages may migrate at the same time toward the neuron clusters (Figure 8e).

Simultaneously migrating clones can encompass different cell numbers, even if they are in the same portion of a stream (e.g., Figure 8a,b). Further, if taking nuclear eccentricity as an indicator for the migration speed of cells (spherical vs. oval-elongate nuclei; see Zhang et al., 2009), different clones may even vary in their migration speed (Figure 8a). These differences illustrate a certain developmental variability between newly generated NP lineages, as opposed to a spatio-temporally invariant cell division cascade.

3.3 | Interaction of hemocytes and other cell types with the adult DPS

3.3.1 | The central niche cavity does not contain cells under basic experimental conditions

To determine whether the central niche cavity may act as a gateway for the integration of hemocytes under basic experimental conditions, we checked for the presence of cells (positive nuclear labeling) in the uncompressed cavity lumen of our 3d virtual stacks. Owing to the applied phalloidin staining and/or tubulin immunolabeling the dimensions of the lumen could be unequivocally assessed (see Figure 1c,d). Notably, out of all niches documented in 3d image stacks, not a single one contained a nucleus (e.g., Figure 1c,d; Table 2). Also among the additional niches that were checked with cLSM but eventually not imaged (>500 DPS processed in total), no nuclei were found in the cavity lumen. Given this considerable number of niches analyzed, this finding is unlikely to be a sampling artifact and suggests that hemocytes do not enter into the cavity lumen under basic conditions, regardless of animal size or the treatment used in the current studies.

3.3.2 | Adoptive transfer experiments result in proliferation marker-labeled cells in the niche

To further study and confirm direct interactions between hemocytes and the DPS under basic conditions, we performed a series of adoptive transfer experiments, in which hemolymph of BrdU- or EdU-exposed donors was injected into recipient animals (see also Benton et al., 2014 for rationale and further details). A total of 115 recipients (58 BrdU and 57 EdU recipients; 224 DPSs intact after dissection) were analyzed, having been subjected to varying post-transfer times prior to sacrifice (see Section 2).

The number of recipients with marker-labeled cells in their DPSs was very low. While none of the BrdU recipients showed positive labeling, three niches of EdU recipients contained labeled cells (~1.5% of 224 recipient niches studied) but no labeled nuclei were observed along the streams. One of the niches with positive labeling was encountered in a recipient sacrificed 3 days after the transfer, whereas the remaining two niches were found in one specimen sacrificed 3 weeks after transfer. Notably, these niches did not contain single but multiple weakly labeled nuclei in their outer cell layers as well as in their core (Figure 10a,b). The morphology of these labeled cells is not distinguishable from adjacent unlabeled Type 1 niche cells, featuring the typical nuclear size and shape.

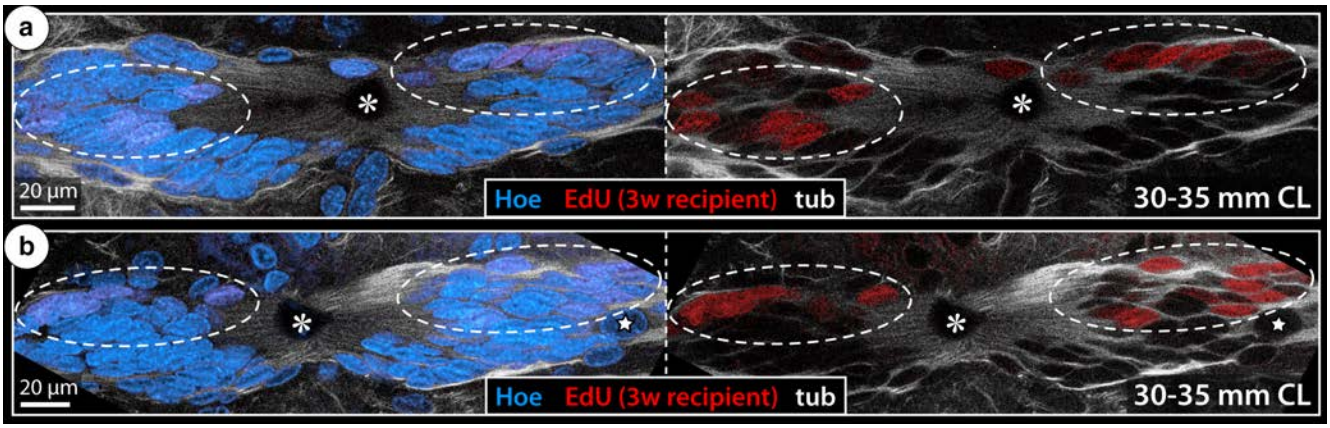

FIGURE 10 EdU-labeled Type 1 cells in the niche following adoptive transfer. (a,b) Optical sections through the two niches of a recipient animal (Imaris oblique slicers), 3 weeks after adoptive transfer. Acetylated tubulin immunolabeling (white) coupled to EdU detection (red) and nuclear counterstain (blue). Carapace length (CL) as indicated in each image. Asterisks mark the central niche cavity. Stippled ovals highlight regions with EdU-positive nuclei. (a) Several Type 1 cell nuclei in each niche half show weak EdU labeling. Note that some of the labeled nuclei are clustered together, indicating their possible derivation from replenishment divisions in the niche. (b) Several partly clustered Type 1 cell nuclei label weakly for EdU in both niche halves. Note the roundish but EdU-negative nucleus of an enlarged first generation NP (star) in one niche half [Color figure can be viewed at wileyonlinelibrary.com]

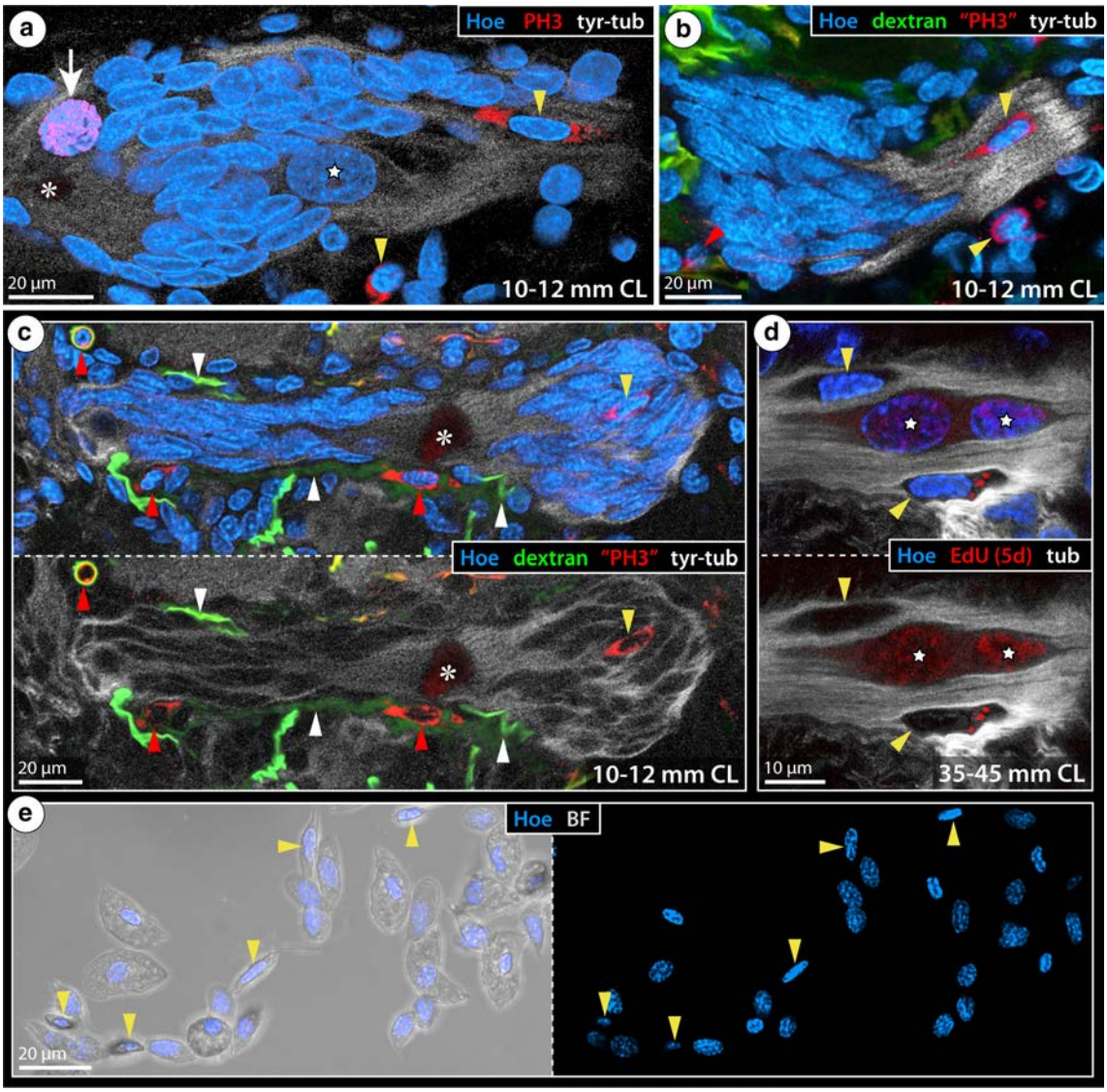

FIGURE 11 Additional cell types of unidentified nature in the DPS. (a–d) Optical sections through niches and/or migratory streams (Imaris oblique slicers). If not (fully) included in the image, the niche with central cavity (asterisk) is located to the left, i.e., NPs migrate toward the right. Acetylated or tyrosinated tubulin immunolabeling (white) coupled to nuclear counterstain (blue). Specimens in a–c also immunolabeled for phospho-histone H3 (PH3, red) and injected with dextran (green, if shown). Carapace length (CL) as indicated in each image. Stars mark nuclei of migrating NPs. (a) Detail of a niche cell cluster half. Note PH3-positive mitotic profile (arrow) next to the cavity. Two cells with small nuclei and cytoplasmic "PH3"-signal are located right next to the niche (lower yellow arrowhead) and at the niche-stream boundary in the DPS (upper yellow arrowhead). (b) Detail of a niche cell cluster half and the proximal stream portion. Note dextran-labeled vasculature next to the cell cluster and stream and a cell with cytoplasmic "PH3"-signal associated with it (red arrowhead). Two further cells with cytoplasmic label are found next to and within the stream (yellow arrowheads). (c) Overview of niche that is closely surrounded by dextran-labeled vasculature (highlighted by white arrowheads). Note the presence of small cells with cytoplasmic "PH3"-signal in the niche cell cluster (yellow arrowhead) and in the vasculature (red arrowheads). (d) Detail of a stream of an adoptive transfer donor, 5 days after exposure to EdU (red). Nuclei of a pair of migrating NPs show very weak EdU label (see lower image). Two unidentified smaller cells with elongate nuclei (yellow arrowheads) are found in the outer edges of the stream. Note complete absence of EdU signal in their nuclei (lower image) and some EdU-labeled granules/vesicles in the cytoplasm of one of them. (e) Optical section of hemocytes obtained from an adoptive transfer donor. Brightfield microscopy (left) and fluorescent nuclear counterstain (blue). Some of the smaller hemocytes circulating in the hemolymph feature a small elongate nucleus (yellow arrowheads) and tiny cytoplasmic cell processes [Color figure can be viewed at wileyonlinelibrary.com]

3.3.3 | Further cell types of unresolved nature in the DPS

Immunolabeling of phosphorylated histone H3 resulted not only in the expected DNA-associated staining in mitotic profiles (arrows in Figures 3e and 11a) but also in nonspecific labeling of the cytoplasm of some cells in the niche and streams (yellow arrowheads in Figure 11a–c). These cells often possess short cytoplasmic processes on both sides of the nucleus. In addition, the nuclei are frequently smaller and even more elongate than most Type 1 cell nuclei and are

intensely Hoechst-stained (Figure 11a,b). Occasionally, the nucleus may also have a conspicuous blunt end on one side (e.g., Figures 9d and 11d). Based on these nuclear characteristics, such cells could be identified even without the nonspecific cytoplasmic labeling in the streams (yellow arrowheads in Figures 6c,f, 7e, 8a, 9a,c,d and 11d), where they occur mostly singly—rarely also in pairs—but never in conspicuous linear arrays as the NP clones. Further, these cells also did not label for proliferation markers in any of our experiments (e.g., Figures 7e and 11d), indicating that they are either cycling very slowly or already postmitotic. To date, the exact nature of this cell type is unclear.

Interestingly, however, cells with identical nonspecific cytoplasmic labeling and nuclear morphology were also found near the surface of the DPS (Figures 3e and 11a–c) and more widely dispersed in other brain areas (not shown). In dextran-injected animals, some of them were revealed to be located inside the arterioles around the niche (red arrowheads in Figure 11b,c), which points toward hemocytes circling in the brain's vasculature. Additional tentative support for this notion may come from the study of the hemolymph of *P. clarkii*. Among the different hemocytes, small elongated cells with short processes, an intensely labeled nucleus and a relatively homogeneous nongranular cytoplasm are found (Figure 11e).

4 | DISCUSSION

4.1 | Intrinsic cell divisions contribute to the replenishment of the niche cell pool

Previous studies have shown that only few in vivo proliferation marker-labeled cells are found in the niche of *P. clarkii* at any given time point within the first post-exposure days (e.g., Benton et al., 2011; Song et al., 2009; Sullivan et al., 2007). Further, mitotic profiles have been observed even more rarely (Song et al., 2009; Sullivan et al., 2007; Zhang et al., 2009) and when captured in a late stage of mitosis (ana- or telophase), they were located close to the niche-stream boundary with a division plane perpendicular to the niche-stream axis (Zhang et al., 2009). This is in line with the NP divisions described here. However, we found additional mitoses next to the cavity lumen among the short processes of Type 1 cells that have not been documented before. Their location opposite to the stream and the orientation of their division planes perpendicular to the surface of the cavity lumen speaks against an immediate migration of the two prospective daughter cells into the streams. Moreover, the occurrence of these divisions in animals of all size groups studied (with a possible trend of a size-dependent decrease, Table 2) and across different experimental setups prior to sacrifice (Table 1) demonstrates that their presence is neither restricted to a certain animal age nor strictly treatment-dependent. Instead, they seem to be a characteristic feature of the DPS in adult crayfish. The observation that these mitotic cells extend processes toward the cavity and into the stream indicates that they represent cycling bipolar Type 1 niche cells.

As the niche is composed of more cells with increasing animal size (Zhang et al., 2009), there needs to be a mechanism driving this rise in niche cell numbers. Apart from the attraction and integration of extrinsic cells (Benton et al., 2011, 2014; see below), intrinsic multiplication via niche cell divisions is another possible mechanism that has, however, not been previously observed (Zhang et al., 2009). The mitoses next to the cavity described here fit such an intrinsic cell amplification mechanism, being locally separated from the differently oriented neurogenic divisions of the first generation NPs. Accordingly, we propose that the symmetric Type 1 cell divisions adjacent to the cavity constitute one of the processes by which the niche cell pool is replenished in the crayfish DPS (see below, Figure 13).

4.2 | The crayfish DPS: A pseudostratified neuroepithelium with INM-like dynamics?

Similarities between these replenishment divisions next to the cavity and cell divisions in the neuroectoderm of other metazoan taxa become more apparent, when recognizing the epithelial-like nature of the crayfish DPS. On first glance, this epithelial-like character is masked by the extreme elongation of the Type 1 cell processes and the clustering of the majority of nuclei in the niche region (Figure 12a). However, the cavity is surrounded by the short Type 1 cell processes, which in an ultrastructural investigation have been shown to be tightly connected to each other by septate junctions and *zonulae adherens* (Chaves da Silva et al., 2012). In line with this, the cell processes exhibit strong immunolabeling for N-cadherin (Sullivan et al., 2007), a member of the cadherin transmembrane glycoprotein family that is a key player in cell–cell adhesion (among other functions). The cytoplasmic domain of cadherins binds via additional protein complexes to cytoskeletal actin filaments (e.g., Mège & Ishiyama, 2017), which we here revealed by phalloidin labeling to be highly concentrated in the tips of the Type 1 cell processes. As pointed out before (Chaves da Silva et al., 2012), these cell–cell contacts in the niche are characteristic features of the apical side of epithelia.

Thus, in a thought experiment, opening and straightening of the curved cavity of each niche half would create the apical side a planar epithelium (Figure 12b). Similarly, hypothetical shortening of the stream portion would result in a more readily recognizable single-layered polarized epithelium, consisting of Type 1 cells whose nuclei are located at different apico-basal levels in a pseudostratified arrangement (Figure 12b). One of the characteristic features of pseudostratified epithelia in various metazoan taxa is the phenomenon of interkinetic nuclear migration (INM) of cycling cells (e.g., Bone & Starr, 2016; Meyer, Ikmi, & Gibson, 2011; Strzyz et al., 2015). During INM, the nucleus migrates apically in G2 phase, passes through M phase near the epithelium's surface and returns further basally during G1 phase. If the cavity's surface is defined as apical side of the neuroepithelium, the location of a considerable portion of mitoses near this surface is reminiscent of INM and may point to similar coupling between nuclear migration and cell cycle in the replenishment divisions of Type 1 cells (i.e., apical migration during G2, M phase and cytokinesis next to the cavity, basally directed migration of daughter cells back into the niche

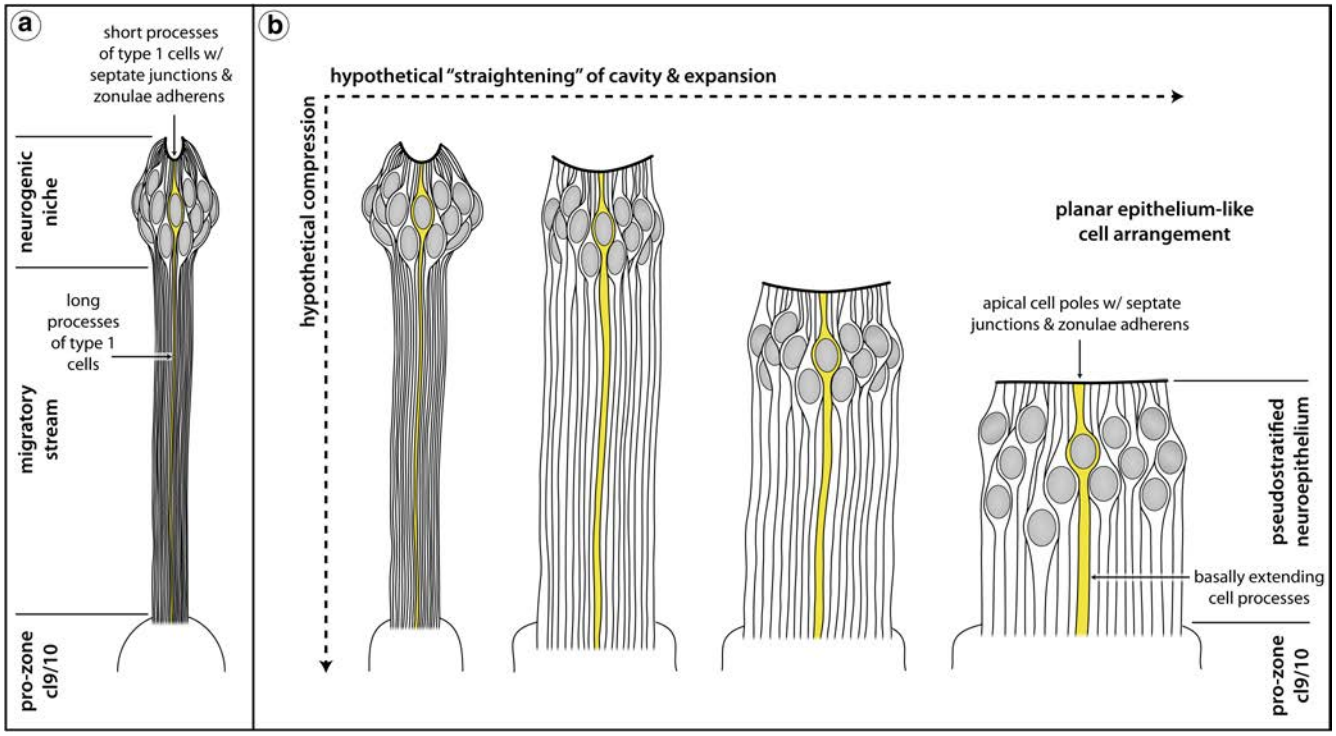

FIGURE 12 Hypothetical transformation of the DPS into a planar pseudostratified neuroepithelium. (a) Semi-schematic representation of one half of the adult DPS with its three sub-regions, the neurogenic niche, migratory stream and the proliferation zone toward Cluster 9 or 10 (pro-zone cl9/10). One bipolar Type 1 niche cell is highlighted in yellow. (b) Hypothetical transformation of the DPS into a planar pseudostratified neuroepithelium via (a) straightening of the niche half's cavity and expansion along the thus created planar arrangement of apical cell poles as well as (b) compression of the extremely long Type 1 cell processes. Note that ultrastructural details on the—now basal—proliferation zones and the surrounding neuron clusters are still unknown (e.g., presence/absence of a basement membrane) [Color figure can be viewed at wileyonlinelibrary.com]

cell cluster; Figure 13a). As of now, however, it remains unresolved if such INM-like divisions are repeated by the Type 1 cells (i.e., self-renewing divisions) or if they rather represent a one-time event with subsequent differentiation of one or both daughter cells into enlarged active NPs. Previous proliferation marker retention experiments speak for the limited mitotic activity of cells prior to niche exit, as BrdU and EdU labels are retained in niche cells only for short time periods (e.g., Benton et al., 2011; Sullivan et al., 2007). Nevertheless, clarification via live imaging would provide irrefutable evidence.

4.3 | Bipolar niche cells differentiate into proliferating first generation NPs

In addition to mitoses near the cavity that contribute to the replenishment of the niche cell pool, we also confirmed divisions of the enlarged first generation NPs with cleavage planes oriented roughly perpendicular to the niche-stream axis (e.g., Song et al., 2009; Zhang et al., 2009). However, deviating from previous reports (Zhang et al., 2009), we found that late mitotic phases and cytokinesis of these NP divisions are not restricted to the niche-stream boundary but may also occur centrally in the niche cell cluster4. We could further confirm that first generation NPs actively in the cell cycle can be morphologically identified based on their larger, more spherical nucleus and a more voluminous cytoplasmic compartment than the surrounding Type 1 niche cells (Song et al., 2009). The less intense labeling of the large NP nuclei with fluorescent nuclear stains suggests predominantly euchromatic as opposed to heterochromatic DNA. Interestingly, all of these features fit well with the histological and ultrastructural features of Type 2 niche cells (Zhang et al., 2009; Chaves da Silva et al., 2012), which we propose to represent the active first generation NPs in the niche.

In contrast to the findings of Song et al. (2009) and to results in spiny lobsters and non-reptant decapod crustaceans (Schmidt, 2007; Schmidt & Derby, 2011; Wittfoth & Harzsch, 2018), we did not detect an enlarged NP in every crayfish DPS studied. In fact, a substantial portion of our 3d-analyzed samples lacked this morphologically conspicuous cell type (Table 2). Together with previous results of proliferation marker retention studies (Benton et al., 2011, 2014; Sullivan et al., 2007), this contradicts theories of a permanently enlarged neural stem cell (i.e., a large adult neuroblast) at the base of adult-born lineages in crayfish. In our current study, the cell projections extending from dividing first generation NPs and their two daughter cells toward the cavity and into the streams favor instead their derivation from bipolar Type 1 cells that have entered the cell cycle. This is also consistent with the separate "lanes" along which the different cell clones migrate through the DPS streams: with a Type 1 cell that differentiates into an active first generation NP as

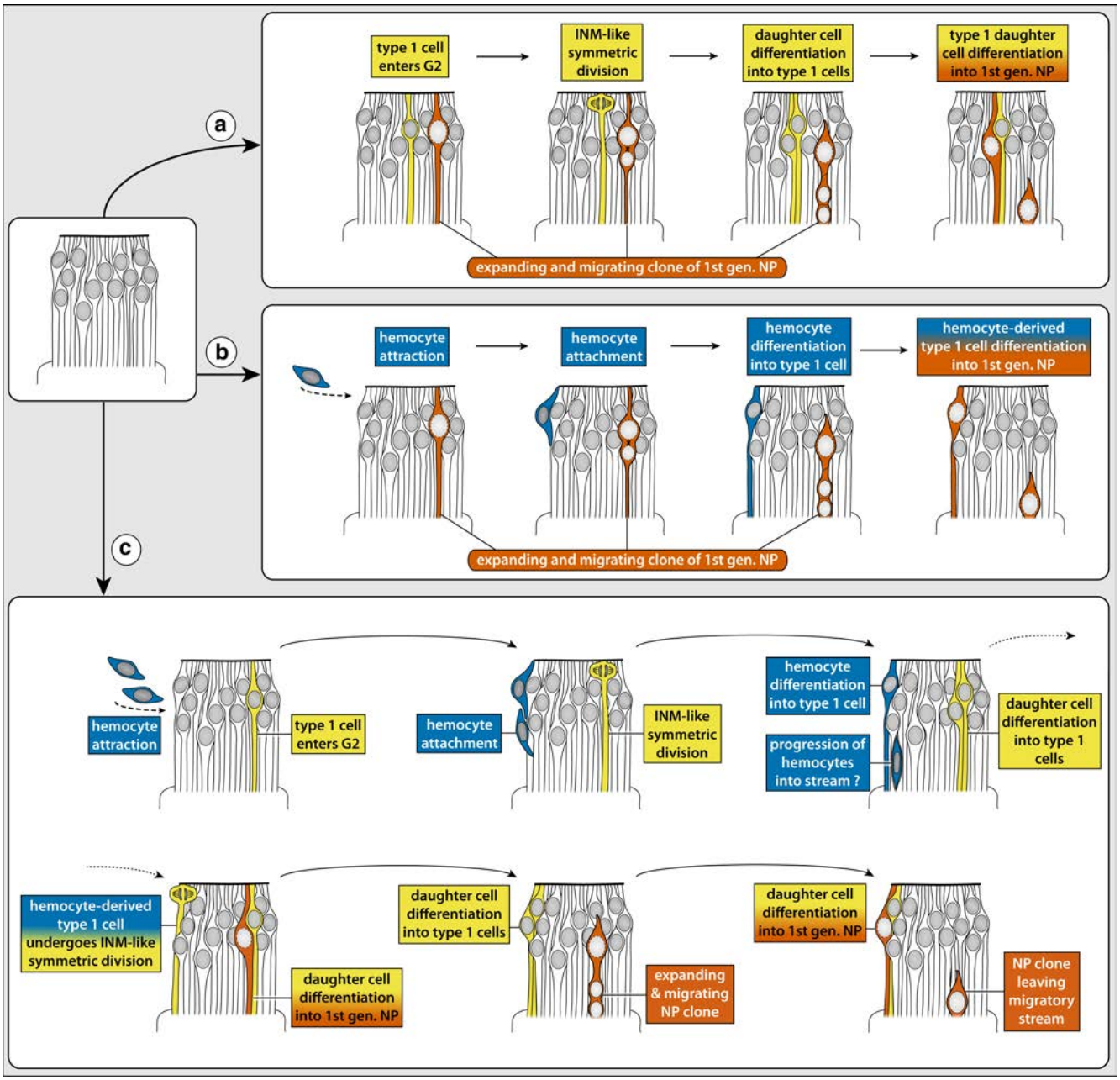

FIGURE 13 Different mechanisms of niche cell pool replenishment. Continuous cell loss in the niche due to the migration of activated first generation neural progenitors (NPs) and their expanding lineages (highlighted in vermillion) can be compensated for by different mechanisms. See Figure 12 for orientation of the neuroepithelium. (a) Intrinsic replenishment in the niche cell pool. Type 1 niche cells (highlighted in yellow) undergo symmetric replenishment divisions. The M phase of these divisions occurs next to the cavity lumen (= apical side of the hypothetical planar neuroepithelium), which is reminiscent of interkinetic nuclear migration (INM) in pseudostratified epithelia. Both daughter cells remain in the niche cell cluster, but may later differentiate into NPs that give rise to a migrating NP lineage. (b) Niche cell pool replenishment via an extrinsic source (modified from Benton et al., 2011, 2014). Hemocytes (most likely of the semi-granular type) attach and integrate into the niche cell cluster, where they differentiate into Type 1 cells (highlighted by blue shading) and may later on turn into enlarged NPs. (c) Niche cell pool replenishment via extrinsic source *and* intrinsic divisions. Attachment and integration of hemocytes into the niche cell clusters (blue shading) coupled to symmetric replenishment divisions (yellow) counteract and even overcompensate for the depletion of the niche cell pool to provide cellular material for life-long NP specification and migration (vermillion). Potentially, hemocyte-derived Type 1 cells undergo one or more symmetric replenishment divisions as well (to date, the exact sequence of divisions is still unknown). Further, single hemocytes may show different types of interactions with the DPS and progress as single cells through the streams [Color figure can be viewed at wileyonlinelibrary.com]

the origin of each clone, its long process in the stream may predict the specific migration lane and act as a migration guide from the onset of clone expansion.

4.4 | Migrating clones encompass different cell generations and include transit-amplifying intermediate NPs

String-like arrangements of NPs as they migrate toward the proliferation zones have been previously documented (e.g., Sullivan et al., 2007; Zhang et al., 2009), but the common lineage of cells linearly aligned along the streams was not recognized. Prior to the current study, the model for the adult NP lineages in crayfish assumed that three NP generations occur spatially separated along the DPS (e.g., Benton et al., 2011, 2014; Zhang et al., 2009). Our new data lead to several modifications of this model.

1. Deviating from earlier descriptions (Zhang et al., 2009), we identified slight morphological asymmetries in divisions of the first generation NPs. Morphologically asymmetric divisions are a typical feature of the neural stem cells (neuroblasts) that lie at the base of embryonic and larval neurogenesis in insects (Doe & Goodman, 1985; Hartenstein, Rudloff, & Campos-Ortega, 1987; Homen & Knoblich, 2012; Tamarelle, Haget, & Ressouches, 1985; Truman & Ball, 1998; Urbach & Technau, 2003) and various crustaceans (Dohle, 1976; Harzsch, 2001; Hein & Scholtz, 2018; Ungerer, Eriksson, & Stollewerk, 2011; Ungerer & Scholtz, 2008) including crayfish (e.g., Scholtz, 1992; Sintoni et al., 2012; Sullivan & Macmillan, 2001). Notably, this morphological asymmetry can be very pronounced in some taxa, whereas it is less obvious in others (e.g., Harzsch, 2001; Hein & Scholtz, 2018) and may additionally decrease with ongoing development (e.g., Homen & Knoblich, 2012). Further, while morphological asymmetry of two newly forming NP daughter cells is one indicator for their non-equivalence, it does not per se suffice to prove long-term self-renewal of the parent NP, as expected for a bona fide stem cell. In the case of the DPS in adult crayfish, we concur with earlier findings that no long-term self-renewing stem cells reside in the niche (Benton et al., 2011). This view is supported by (a) the absence of an enlarged cell (= potential adult neuroblast) in a significant portion of the niches studied, (b) the observed cell division and migration patterns, and (c) the absence of in vivo cell proliferation marker retention in the niche cell pool for even few days after a marker pulse (e.g., Benton et al., 2011, 2014). Instead, the entire progeny of a first generation NP exits the niche. But in contrast to the previous DPS model, the first generation NPs may divide more than once prior to their niche exit (see Figure 6a) and very likely continue to do so for some time as they migrate at the tail end of expanding clones (proximal to the niche). Accordingly, the tail-end NPs rather qualify as a type of intermediate NP (INP) with limited short-term proliferative potential. This is reminiscent of the specialized NP lineages that form the central complex in the brain of *Drosophila* and grasshoppers, where transit-amplifying INPs with short-term self-renewal capacity lead to a significant amplification of these lineages compared to other neural lineages in the brain (Bello, Izergina, Caussinus, & Reichert, 2008; Boyan & Williams, 2011; Homen & Knoblich, 2012). The observed slight enlargement of the tail-end INPs in clones traversing the DPS may be related to their growth in the G phases prior to S phase and mitosis, respectively.

2. The previous DPS model included migrating cells (then interpreted as second generation NPs) that may occasionally pass through M phase in the streams and migrate often as sister cell pairs (Zhang et al., 2009). Our new data add significantly to this model because they reveal that not pairs but multicellular groups of clonally related cells migrate through the streams in linear arrays, continuing to expand while doing so. In addition to divisions of the tail-end INP, further divisions of its daughter cells closer to a clone's migration front contribute to lineage expansion. Similar to the tail-end INP, the occasional enlargement of some nuclei in the middle of a clone likely correlates with the growth of cycling cells during one of the G phases. To date, however, we are unable to determine, if all daughter cells of a tail-end INP divide again and whether they do so according to a stereotyped mode (e.g., just once like typical embryonic ganglion mother cells; see Ungerer & Scholtz, 2008). Nevertheless, the observation of simultaneously migrating clones next to each other in the streams and their deviating cell numbers speaks strongly for a spatio-temporally flexible rather than an invariant cell division pattern. Moreover, not only the cell number but also the distance between nuclei and their shape can show considerable variations between and even within clones (see also Zhang et al., 2009). This suggests temporally dynamic nucleus/cell migration speeds, with similarities to saltatorial nucleokinesis during neuronal migration in vertebrates (Marín, Valiente, Ge, & Tsai, 2010; Tsai & Gleeson, 2005). As a consequence of these various dynamic processes, cells observed at any given time point in the streams are likely to represent a mixture of different NP generations that can belong to separate adult NP lineages.
3. In the proliferation zones within the neuron clusters, we are still unable to reliably discriminate between different adult NP lineages with the available morphological toolkit. This basal-most region of the crayfish DPS frequently features mitotic profiles, which have been previously assigned to third generation NPs (Zhang et al., 2009). In our revised DPS model, it might be more fittingly said to be a clone accumulation area, in which different NP generations of still expanding lineages become spatially packed prior to cell cycle exit and neuronal differentiation.

4.5 | Where do hemocytes integrate into the DPS?

Interactions between the DPS and hemocytes of the innate immune system have been a focus in previous studies. Injection of fluorescently labeled dextran into the dorsal sinus revealed an intimate

spatial association of the niche and brain vasculature and even indicated direct communication of the hemolymph with the niche cavity (Sullivan et al., 2007; Chaves da Silva et al., 2012, 2013). Moreover, in-vitro experiments showed that one hemocyte type (semi-granular cells) is selectively attracted to and attaches to the niche (Benton et al., 2011). This intriguing finding was then further explored in vivo via adoptive transfer experiments. Here, hemolymph of proliferation marker-exposed donor animals was injected into untreated recipient animals, which resulted in the appearance of labeled cells in recipient niches, migratory streams and Clusters 9 and 10 after different post-transfer time periods, coupled to their neurotransmitter expression in the clusters which is indicative of neuronal differentiation (Benton et al., 2014). Up to now, however, it is unclear which local area of the niche acts as gateway for hemocyte integration and the cavity has been discussed as one of the possible options (Benton et al., 2011, 2014).

However, our 3d analysis of more than 200 imaged niches does not point toward the cavity as important hemocyte entry into the DPS. In fact, we did not find a single instance of a nucleus inside the clearly demarcated central lumen, whereas hemocyte nuclei were readily observed in the vasculature and sinus spaces in direct vicinity to the niche and in other brain areas. Based on our large sample size, we therefore assume that hemocytes only rarely—if ever—enter into the cavity under basic conditions. Alternatively, attachment to the ventral and dorsal niche surfaces seems a more plausible route for hemocyte integration. Indeed, this type of surface attachment was observed in vitro (Benton et al., 2011). The niche surfaces lack any surrounding barriers, such as a basement membrane, which would impede direct cell–cell attachment (Chaves da Silva et al., 2012). Further, their larger area compared to the small cavity surface may allow integration of more cells in a shorter time period. Such notable increases in cells associated with the niche have been observed when the system is perturbed, for example by exposure to increased levels of serotonin or astakine (Benton et al., 2011, 2014). The mechanisms by which hemocytes are attracted to the niche and integrate into the cell cluster under varying conditions are not known and await the ability to examine these questions with live-imaging approaches.

In spite of the low success rate of our adoptive transfer experiments, the niches that did show positive proliferation marker labeling clearly support such hemocyte integration into the niche (see also Benton et al., 2014). Notably, we found multiple labeled cells with typical nuclear morphology of Type 1 cells in the niche cell clusters 3 weeks after hemocyte transfer. This indicates either (a) separate integration of many hemocytes or (b) integration of few hemocytes and their subsequent amplification via replenishment divisions (see below; Figure 13c). Such additional divisions could explain the relatively low intensity of the marker signal, as it would have been increasingly diluted with each mitosis. Future experiments will need to decipher in more detail which endogenous and exogenous factors may impact the frequency and extent of hemocyte integration into the DPS and thus the success rate of adoptive transfers.

4.6 | Niche replenishment: A balance of hemocyte integration and niche cell proliferation

When combining our results on cell divisions and migration patterns with the available adoptive transfer results, we currently favor an extended niche replenishment model (Figure 13c). It includes the previously reported integration of hemocytes (Figure 13b; Benton et al., 2014) but further adds their likely differentiation into bipolar Type 1 cells (as suggested by adoptive transfer experiments) as well as the occurrence of symmetric replenishment divisions among Type 1 cells (as implied by the INM-like mitoses next to the cavity; Figure 13a). Under this extended model, the synergistic effect of extrinsic cell integration and intrinsic replenishment divisions compensates for the constant efflux of NPs from the niche cell pool. As the niche cell number increases with animal size (Zhang et al., 2009), these two processes even seem to overcompensate for the cell efflux during an animal's lifetime.

Interestingly, previous adoptive transfer experiments (Benton et al., 2014) resulted in single labeled cells in the migratory streams. Given our observation of single cells with hemocyte-like morphological characteristics and low proliferation activity in the streams, this may hint toward additional cell migration processes not related to the adult NP lineages (Figure 13c). As of now, the identity of the cells with nonspecific cytoplasmic labeling after PH3 immunohistochemistry remains unresolved and needs further investigation. An alternative to the hemocyte identity we have suggested here is their potential glial nature. Pointing in this direction, similar cytoplasmic labeling of a PH3 antibody was reported in the brains of spiny lobsters (Schmidt & Derby, 2011), where the cells were interpreted as glia due to their multipolar processes.

4.7 | DPS similarities to neuroepithelia in the development of non-insect arthropods

In several non-insect arthropods, the neuroectoderm of advanced developmental stages (embryonic or postembryonic) resembles a pseudostratified epithelium. In line with the potential occurrence of INM-like dynamics, neuroepithelial cell divisions with apical mitoses compensate here for the loss of cell material as a result of basal migration and internal detachment of cells that have committed to the neural pathway (e.g., Stollewerk, Weller, & Tautz, 2001 [spiders]; Dove & Stollewerk, 2003 [millipedes]; Brenneis et al., 2013 [sea spiders]). Moreover, specific areas of the neuroepithelium may invaginate and detach from the surface during late embryonic development of these taxa, to persist temporarily or throughout the animal's life as cell clusters at the surface of or within the underlying ganglionic somata cortex (Brenneis et al., 2013; Brenneis & Scholtz, 2014; Brenneis, Scholtz, & Beltz, 2018; Döffinger, Hartenstein, & Stollewerk, 2010; Dohle, 1964; Pioro & Stollewerk, 2006; Stollewerk, 2004). These internalized epithelial cell clusters continue to produce additional cells for the differenti-

ating central nervous system. Notably, the invagination processes leading to the clusters affect neither the spatial arrangement of neighboring cells to each other nor the apico-basal polarization laid down during embryonic ectoderm development. As a consequence, the previously outward facing apical cell poles are directed toward the center of the clusters and converge around a tiny central cavity in an arrangement very similar to the crayfish niche. In some sea spiders, fibrous bundles of elongate cell processes also emanate from these neurogenic clusters into the soma cortex and have been shown to act as a migration pathway for newborn cells into the ganglion (Brenneis et al., 2018; Brenneis & Scholtz, 2014). Given these structural and functional similarities to the crayfish DPS, it would not be surprising if the latter was likewise formed via ectodermal invagination in late embryonic stages, with a retention of the apico-basal polarization. So far, however, the developmental origin of the DPS remains elusive, as the available studies started either too late in development (Song et al., 2009) or were not focused on the potential relationship between apical embryonic ectoderm and emerging DPS (Sintoni et al., 2012).

4.8 | Cell fate switch as in the *Drosophila* optic lobe and the mammalian neocortex?

In the simplified planar DPS model, the spindles of the apical replenishment divisions are aligned in parallel to the epithelial surface (Figure 13a,c). This closely resembles the symmetric proliferative divisions of neuroepithelial cells in the optic lobe of *Drosophila* and the developing mammalian cerebral cortex (e.g., Brand & Livesey, 2011). Likewise, the proposed transformation of Type 1 niche cells into the active first generation NPs is similar to these two model systems, in which progeny of symmetrically dividing epithelial cells transform into repeatedly dividing NPs (neuroblasts and radial glial cells, respectively). As in the crayfish DPS, this is accompanied by a change of their spindle orientation (from parallel to oblique/perpendicular to the surface). In mammals, this changed spindle orientation has been even implicated to cause the switch from proliferative divisions to the neurogenic NP division mode (Xie, Jüschke, Esk, Hirotsune, & Knoblich, 2013). However, in the optic lobe of *Drosophila*, experimentally induced change of spindle orientation is not sufficient for transformation into an NP (Egger, Boone, Stevens, Brand, & Doe, 2007). Instead, transient repression of members of the Notch signaling pathway via the proneural gene *lethal of scute* of the *achaete-scute* transcription factor family has been shown to promote NP differentiation in a restricted area of the epithelium (Egger, Gold, & Brand, 2010). This interplay of spatio-temporally tightly regulated proneural gene expression and Notch signaling is an evolutionarily conserved mechanism governing neural commitment of epithelial cells in the development of various arthropod groups (Skeath & Thor, 2003; Wheeler, Carrico, Wilson, Brown, & Skeath, 2003; Kux, Kiparaki, & Delidakis, 2013 [insects]; Stollewerk et al., 2001; Stollewerk, 2002 [spiders]; Dove & Stollewerk, 2003; Kadner & Stollewerk, 2004 [myriapods]) and many other taxa, including vertebrates (see Hartenstein & Stollewerk, 2015). Accordingly, a similar molecular switch may be key for the selection of single Type 1 niche cells and their differentiation into first generation NPs in the crayfish DPS. Gene expression studies that seek to explore this aspect are currently underway.

4.9 | Parallels with neurogenesis in the adult mammalian brain

In the adult mammalian brain, neurogenesis occurs in two principal regions, the subventricular zone (SVZ) in the wall of the lateral ventricle and the subgranular zone (SGZ) of the dentate gyrus. Adult neurogenesis was initially believed to be sustained by long-term self-renewing NPs that reside in the both regions (B1 cells in the SVZ; radial glia-like cells [R-cells] in the SGZ) and undergo predominantly asymmetric divisions in stem cell-like manner. In the meantime, however, this has turned into a matter of debate (e.g., Bond, Ming, & Song, 2015) and an increasing body of evidence indicates considerable heterogeneity among the primary adult NPs, many of which appear to lack a capacity for long-term self-renewal and become quickly exhausted once activated (Calzolari et al., 2015; Encinas et al., 2011; Fuentealba et al., 2015; Pilz et al., 2018). A recent study now even suggests that neurogenesis in the SVZ is not even driven by asymmetric divisions of the B1 cells (Obernier et al., 2018). Instead, the majority of them were observed to undergo symmetric consuming divisions that generate two transit-amplifying NPs and thus deplete the B1 cell pool, whereas the remaining smaller fraction passes through *symmetric* self-renewal, producing two B1 cells. Similarly, a live-imaging study on the SGZ has documented only limited self-renewal of R-cells via asymmetric but also symmetric divisions, prior to their exhaustion in consuming neurogenic divisions (Pilz et al., 2018). Notably, asymmetric self-renewal divisions were observed to follow on symmetric ones but never vice versa, thus showing similarities to cortical development during which NPs irreversibly transition from a symmetric proliferative to an asymmetric neurogenic phase.

These novel insights into the cellular dynamics of mammalian adult neurogenesis feature again some remarkable parallels to our proposed crayfish DPS model (Figure 13c), where bipolar Type 1 niche cells may undergo symmetric proliferative divisions before transforming into first generation NPs that in turn enter consuming neurogenic divisions and give rise to clones of migrating NPs with finite proliferation potential. These parallels between the life-long neurogenic mechanisms of two taxa as phylogenetically distant as crayfish and mammals may serve as another illustration of how evolution independently generates similar solutions when faced with similar challenges. Seen from this perspective, the recently discovered novel mode of NP pool replenishment via integration and neural differentiation of hemocytes in the crayfish DPS (Benton et al., 2014) may well represent a more ubiquitous pathway than originally appreciated and thus inform the future direction of studies on mammalian systems (see Beltz et al., 2015; Beltz, Brenneis, & Benton, 2016 for further discussion).

ACKNOWLEDGMENTS

We are deeply indebted to Jeanne L. Benton for her expert advice in all matters concerning crayfish experiments and for her help during a first round of adoptive transfer experiments. Pat Carey and Valerie

LePage are thanked for care of the animals used in the studies. GB received funding from the Deutsche Forschungsgemeinschaft (DFG; grant-nos. BR5039/1-1, BR5039/3-1). The project was supported by a National Science Foundation grant to BSB (NSF-IOS-1656103).

DATA AVAILABILITY STATEMENT

The data that support the findings of this study are available from the corresponding author upon reasonable request.

ORCID

Georg Brenneis https://orcid.org/0000-0003-1202-1899

REFERENCES

Ayub, N., Benton, J., Zhang, Y., & Beltz, B. (2011). Environmental enrichment influences neuronal stem cells in the adult crayfish brain. *Developmental Neurobiology*, *71*, 351–361.

Bello, B. C., Izergina, N., Caussinus, E., & Reichert, H. (2008). Amplification of neural stem cell proliferation by intermediate progenitor cells in *Drosophila* brain development. *Neural Development*, *3*, 5.

Beltz, B., Cockey, E., Li, J., Platto, J., Ramos, K., & Benton, J. (2015). Adult neural stem cells: Long-term self-renewal, replenishment by the immune system, or both? *BioEssays*, *37*, 495–501.

Beltz, B. S., Brenneis, G., & Benton, J. L. (2016). Adult neurogenesis: Lessons from crayfish and the elephant in the room. *Brain, Behavior and Evolution*, *87*, 146–155.

Benton, J., Goergen, E., Rogan, S., & Beltz, B. S. (2008). Hormonal and synaptic influences of serotonin on adult neurogenesis. *General and Comparative Endocrinology*, *158*, 183–190.

Benton, J., Sandeman, D., & Beltz, B. (2007). Nitric oxide in the crustacean brain: Regulation of neurogenesis and morphogenesis in the developing olfactory pathway. *Developmental Dynamics*, *236*, 3047–3060.

Benton, J. L., Kery, R., Li, J., Noonin, C., Söderhäll, I., & Beltz, B. S. (2014). Cells form the immune system generate adult-born neurons in crayfish. *Developmental Cell*, *30*, 322–333.

Benton, J. L., Zhang, Y., Kirkhart, C. R., Sandeman, D. C., & Beltz, B. S. (2011). Primary neuronal precursors in adult crayfish brain: Replenishment from a non-neuronal source. *BMC Neuroscience*, *12*, 53.

Bond, A., Ming, G.-I., & Song, H. (2015). Adult mammalian neural stem cells and neurogenesis: Five decades later. *Cell Stem Cell*, *17*, 385–395.

Bone, C., & Starr, D. (2016). Nuclear migration events throughout development. *Journal of Cell Science*, *129*, 1951–1961.

Boyan, G., & Williams, L. (2011). Embryonic development of the insect central complex: Insights from lineages in the grasshopper and *Drosophila*. *Arthropod Structure and Development*, *40*, 334–348.

Brand, A. H., & Livesey, F. J. (2011). Neural stem cell biology in vertebrates and invertebrates: More alike than different? *Neuron*, *70*, 719–729.

Brenneis, G., & Scholtz, G. (2014). The 'ventral organs' of Pycnogonida (Arthropoda) are neurogenic niches of late embryonic and post-embryonic nervous system development. *PLoS One*, *9*, e95435. https://doi.org/10.1371/journal.pone.0095435

Brenneis, G., Scholtz, G., & Beltz, B. (2018). Comparison of ventral organ development across Pycnogonida (Arthropoda, Chelicerata) provides evidence for a plesiomorphic mode of late neurogenesis in sea spiders and myriapods. *BMC Evolutionary Biology*, *18*, 47.

Brenneis, G., Stollewerk, A., & Scholtz, G. (2013). Embryonic neurogenesis in *Pseudopallene* sp. (Arthropoda, Pycnogonida) includes two subsequent phases with similarities to different arthropod groups. *EvoDevo*, *4*, 32.

Calzolari, F., Michel, J., Baumgart, E., Theis, F., Götz, M., & Ninkovic, J. (2015). Fast clonal expansion and limited neural stem cell self-renewal in the adult subependymal zone. *Nature Neuroscience*, *18*, 490–492.

Chaves da Silva, P. G., Benton, J. L., Sandeman, D. C., & Beltz, B. S. (2013). Adult neurogenesis in the crayfish brain: The hematopoietic anterior proliferation center has direct access to the brain and stem cell niche. *Stem Cells and Development*, *22*, 1027–1041.

Chaves da Silva, P. G., Benton, J. L., Beltz, B. S., & Allodi, S. (2012). Adult neurogenesis: Ultrastructure of a neurogenic niche and neurovascular relationships. *PLoS ONE*, *7*, e39267. https://doi.org/10.31371/journal.pone.0039267

Chaves da Silva, P. G., Benton, J. L., Sandeman, D. C., & Beltz, B. S. (2013). Adult neurogenesis in the crayfish brain: the hematopoietic anterior proliferation center has direct access to the brain and stem cell niche. *Stem Cells and Development*, *22*, 1027–1041.

Doe, C. Q., & Goodman, C. S. (1985). Early events in insect neurogenesis. I. Development and segmental differences in the pattern of neuronal precursor cells. *Developmental Biology*, *111*, 193–205.

Döffinger, C., Hartenstein, V., & Stollewerk, A. (2010). Compartmentalisation of the precheliceral neuroectoderm in the spider *Cupiennius salei*: Development of the arcuate body, the optic ganglia and the mushroom body. *The Journal of Comparative Neurology*, *518*, 2612–2632.

Dohle, W. (1964). Die Embryonalentwicklung von *Glomeris marginata* (Villers) im Vergleich zur Entwicklung anderer Diplopoden. *Zoologische Jahrbücher der Anatomie*, *81*, 241–310.

Dohle, W. (1976). Die Bildung und Differenzierung des postnauplialen Keimstreifs von *Diastylis rathkei* (Crustacea, Cumacea). II. Die Differenzierung und Musterbildung des Ektoderms. *Zoomorphologie*, *84*, 235–277.

Dove, H., & Stollewerk, A. (2003). Comparative analysis of neurogenesis in the myriapod *Glomeris marginata* (Diplopoda) suggests more similarities to chelicerates than to insects. *Development*, *130*, 2161–2171.

Egger, B., Boone, J., Stevens, N., Brand, A. H., & Doe, C. Q. (2007). Regulation of spindle orientation and neural stem cell fate in the *Drosophila* optic lobe. *Neural Development*, *2*, 1.

Egger, B., Gold, K., & Brand, A. H. (2010). Notch regulates the switch from symmetric to asymmetric neural stem cell division in the *Drosophila* optic lobe. *Development*, *137*, 2981–2987.

Encinas, J., Michurina, T., Peunova, N., Park, J.-H., Tordo, J., Peterson, D., … Enikolopov, G. (2011). Division-coupled astrocytic differentiation and age-related depletion of neural stem cells in the adult hippocampus. *Cell Stem Cell*, *8*, 566–579.

Eriksson, P., Perfilieva, E., Björk-Eriksson, T., Alborn, A.-M., Nordborg, C., Peterson, D., & Gage, F. (1998). Neurogenesis in the adult human hippocampus. *Nature Medicine*, *4*, 1313–1317.

Fuentealba, L., Rompani, S., Parraguez, J., Obernier, K., Romero, R., Cepko, C., & Alvarez-Buylla, A. (2015). Embryonic origin of postnatal neural stem cells. *Cell*, *161*, 1644–1655.

Gage, F., & Temple, S. (2013). Neural stem cells: Generating and regenerating the brain. *Neuron*, *80*, 588–601.

Grandel, H., & Brand, M. (2013). Comparative aspects of adult neural stem cell activity in vertebrates. *Development, Genes and Evolution*, *223*, 131–147.

Hartenstein, V., Rudloff, E., & Campos-Ortega, J. A. (1987). The pattern of proliferation of the neuroblasts in the wild-type embryo of *Drosophila melanogaster*. *Roux's Archives of Developmental Biology*, *196*, 473–485.

Hartenstein, V., & Stollewerk, A. (2015). The evolution of early neurogenesis. *Developmental Cell*, *32*, 390–407.

Harzsch, S. (2001). Neurogenesis in the crustacean ventral nerve cord: Homology of neuronal stem cells in Malacostraca and Branchiopoda? *Evolution and Development*, *3*, 154–169.

Harzsch, S., & Dawirs, R. R. (1996). Neurogenesis in the developing crab brain: Postembryonic generation of neurons persists beyond metamorphosis. *Journal of Neurobiology*, *29*, 384–398.

Harzsch, S., Miller, J., Benton, J., & Beltz, B. (1999). From embryo to adult: Persistent neurogenesis and apoptotic cell death shape the lobster deutocerebrum. *The Journal of Neuroscience*, *19*, 3472–3485.

Hein, H., & Scholtz, G. (2018). Larval neurogenesis in the copepod *Tigriopus californicus* (Tetraconata, Multicrustacea). *Development, Genes and Evolution*, *228*, 119–129.

Homen, C., & Knoblich, J. A. (2012). *Drosophila* neuroblasts: A model for stem cell biology. *Development*, *139*, 4297–4310.

Kadner, D., & Stollewerk, A. (2004). Neurogenesis in the chilopod *Lithobius forficatus* suggests more similarities to chelicerates than to insects. *Development, Genes and Evolution*, *214*, 367–379.

Kim, Y., Sandeman, D., Benton, J., & Beltz, B. (2014). Birth, survival and differentiation of neurons in an adult crustacean brain. *Developmental Neurobiology*, *74*, 602–615.

Kux, K., Kiparaki, M., & Delidakis, C. (2013). The two *Tribolium E(spl)* genes show evolutionarily conserved expression and function during embryonic neurogenesis. *Mechanisms of Development*, *130*, 207–225.

Lin, X., & Söderhäll, I. (2011). Crustacean hematopoiesis and the astakine cytokines. *Blood*, *117*, 6417–6424.

Marín, O., Valiente, M., Ge, X., & Tsai, L.-H. (2010). Guiding neuronal cell migrations. *Cold Spring Harbor Perspectives in Biology*, *2*, a00183. https://doi.org/10.1101/cshperspect.a001834

Mège, R. M., & Ishiyama, N. (2017). Integration of cadherin adhesion and cytoskeleton at *adherens* junctions. *Cold Spring Harbor Perspectives in Biology*, *9*, a028738. https://doi.org/10.1101/cshperspect.a028738

Meyer, E., Ikmi, A., & Gibson, M. (2011). Interkinetic nuclear migration is a broadly conserved feature of cell division in pseudostratified epithelia. *Current Biology*, *21*, 485–491.

Obernier, K., Cebrian-Silla, A., Thomson, M., Parraguez, J., Anderson, R., Guinto, C., … Alvarez-Buylla, A. (2018). Adult neurogenesis is sustained by symmetric self-renewal and differentiation. *Cell Stem Cell*, *22*, 221–234.

Pilz, G.-A., Bottes, S., Betizeau, M., Jörg, D., Carta, S., Simons, B., … Jessberger, S. (2018). Live imaging of neurogenesis in the adult mouse hippocampus. *Science*, *359*, 658–662.

Pioro, H. L., & Stollewerk, A. (2006). The expression pattern of genes involved in early neurogenesis suggests distinct and conserved functions in the diplopod *Glomeris marginata*. *Development, Genes and Evolution*, *216*, 417–430.

Sandeman, D., Benton, J., & Beltz, B. (2009). An identified serotonergic neuron regulates adult neurogenesis in the crustacean brain. *Developmental Neurobiology*, *69*, 530–545.

Sandeman, D. C., Bazin, F., & Beltz, B. S. (2011). Adult neurogenesis: Examples from the decapod crustaceans and comparisons with mammals. *Arthropod Structure and Development*, *40*, 258–275.

Sandeman, R., & Sandeman, D. (2000). "impoverished" and "enriched" living conditions influence the proliferation and survival of neurons in crayfish brain. *Journal of Neurobiology*, *45*, 215–226.

Schmidt, M. (1997). Continuous neurogenesis in the olfactory brain of adult shore crabs, *Carcinus maenas*. *Brain Research*, *762*, 131–143.

Schmidt, M. (2001). Neuronal differentiation and long-term survival of newly generated cells in the olfactory midbrain of the adult spiny lobster, *Panulirus argus*. *Journal of Neurobiology*, *48*, 181–203.

Schmidt, M. (2007). Identification of putative neuroblasts at the base of adult neurogenesis in the olfactory midbrain of the spiny lobster, *Panulirus argus*. *The Journal of Comparative Neurology*, *503*, 64–84.

Schmidt, M., & Derby, C. D. (2011). Cytoarchitecture and ultrastructure of neural stem cell niches and neurogenic complexes maintaining adult neurogenesis in the olfactory midbrain of spiny lobsters, *Panulirus argus*. *The Journal of Comparative Neurology*, *519*, 2283–2319.

Schmidt, M., & Harzsch, S. (1999). Comparative analysis of neurogenesis in the central olfactory pathway of adult decapod crustaceans by *in vivo* BrdU labeling. *Biological Bulletin*, *196*, 127–136.

Scholtz, G. (1992). Cell lineage studies in the crayfish *Cherax destructor* (Crustacea, Decapoda): Germ band formation, segmentation, and early neurogenesis. *Roux's Archives of Developmental Biology*, *202*, 36–48.

Simoes, A., & Rhiner, C. (2017). A cold-blooded view on adult neurogenesis. *Frontiers in Neuroscience*, *11*, 327.

Sintoni, S., Benton, J. L., Beltz, B. S., Hansson, B. S., & Harzsch, S. (2012). Neurogenesis in the central olfactory pathway of adult decapod crustaceans: Development of the neurogenic niche in the brains of procambarid crayfish. *Neural Development*, *7*, 1.

Skeath, J. B., & Thor, S. (2003). Genetic control of *Drosophila* nerve cord development. *Current Opinion in Neurobiology*, *13*, 8–15.

Song, C.-K., Johnstone, L. M., Edwards, D. H., Derby, C. D., & Schmidt, M. (2009). Cellular basis of neurogenesis in the brain of crayfish, *Procambarus clarkii*: Neurogenic complex in the olfactory midbrain from hatchlings to adults. *Arthropod Structure and Development*, *38*, 339–360.

Stollewerk, A. (2002). Recruitment of cell groups through Delta/notch signalling during spider neurogenesis. *Development*, *129*, 5339–5348.

Stollewerk, A. (2004). Secondary neurons are arrested in an immature state by formation of epithelial vesicles during neurogenesis of the spider *Cupiennius salei*. *Frontiers in Zoology*, *1*, 3.

Stollewerk, A., Weller, M., & Tautz, D. (2001). Neurogenesis in the spider *Cupiennius salei*. *Development*, *128*, 2673–2688.

Strzyz, P., Lee, H., Sidhaye, J., Weber, I., Leung, L., & Norden, C. (2015). Interkinetic nuclear migration is centrosome independent and ensures apical cell division to maintain tissue integrity. *Developmental Cell*, *32*, 203–219.

Sullivan, J. M., & Beltz, B. S. (2005). Newborn cells in the adult crayfish brain differentiate into distinct neuronal types. *Journal of Neurobiology*, *65*, 157–170.

Sullivan, J. M., Benton, J. L., Sandeman, D. C., & Beltz, B. S. (2007). Adult neurogenesis: A common strategy across diverse species. *The Journal of Comparative Neurology*, *500*, 574–584.

Sullivan, J. M., & Macmillan, D. L. (2001). Embryonic and postembryonic neurogenesis in the ventral nerve cord of the freshwater crayfish *Cherax destructor*. *Journal of Experimental Zoology*, *290*, 49–60.

Tamarelle, M., Haget, A., & Ressouches, A. (1985). Segregation, division, and early patterning of lateral thoracic neuroblasts in the embryos of *Carausius morosus* Br. (Phasmida: Lonchodidae). *International Journal of Insect Morphology and Embryology*, *14*, 307–317.

Truman, J. W., & Ball, E. E. (1998). Patterns of embryonic neurogenesis in a primitive wingless insect, the silverfish, *Ctenolepisma longicaudata*: Comparison with those seen in flying insects. *Development, Genes and Evolution*, *208*, 357–368.

Tsai, L.-H., & Gleeson, J. (2005). Nucleokinesis in neuronal migration. *Neuron*, *46*, 383–388.

Ungerer, P., Eriksson, B. J., & Stollewerk, A. (2011). Neurogenesis in the water flea *Daphnia magna* (Crustacea, Branchiopoda) suggests different mechanisms of neuroblast formation in insects and crustaceans. *Developmental Biology*, *357*, 42–52.

Ungerer, P., & Scholtz, G. (2008). Filling the gap between identified neuroblasts and neurons in crustaceans adds new support for Tetraconata. *Proceedings of the Royal Society B*, *275*, 369–376.

Urbach, R., & Technau, G. M. (2003). Early steps in building the insect brain: Neuroblast formation and segmental patterning in the developing brain of different insect species. *Arthropod Structure and Development*, *32*, 103–123.

Wheeler, S. R., Carrico, M. L., Wilson, B. A., Brown, S. J., & Skeath, J. B. (2003). The expression and function of the *achaete-scute* genes in *Tribolium castaneum* reveals conservation and variation in neural pattern formation and cell fate specification. *Development*, *130*, 4373–4381.

Wittfoth, C., & Harzsch, S. (2018). Adult neurogenesis in the central olfactory pathway of dendrobranchiate and caridean shrimps: New insights into the evolution of the deutocerebral proliferative system in reptant decapods. *Developmental Neurobiology*, *78*, 757–774.

Xie, Y., Jüschke, C., Esk, C., Hirotsune, S., & Knoblich, J. A. (2013). The phosphatase PP4c controls spindle orientation to maintain proliferative symmetric divisions in the developing neocortex. *Neuron*, *79*, 254–265.

Zhang, Y., Allodi, S., Sandeman, D. C., & Beltz, B. S. (2009). Adult neurogenesis in the crayfish brain: Proliferation, migration, and possible origin of precursor cells. *Developmental Neurobiology*, *69*, 415–436.

Zhang, Y., Benton, J., & Beltz, B. (2011). 5-HT receptors mediate lineage-dependent effects of serotonin on adult neurogenesis in *Procambarus clarkii*. *Neural Development*, *6*, 2.

Zhao, C., Deng, W., & Gage, F. (2008). Mechanisms and functional implications of adult neurogenesis. *Cell*, *132*, 645–660.

SUPPORTING INFORMATION

Additional supporting information may be found online in the Supporting Information section at the end of this article.

How to cite this article: Brenneis G, Beltz BS. Adult neurogenesis in crayfish: Origin, expansion, and migration of neural progenitor lineages in a pseudostratified neuroepithelium. *J Comp Neurol*. 2019;1–27. https://doi.org/10.1002/cne.24820